The First-Order Evolution of Cosmic Scalar Perturbations

master's thesis, 27.9.2019

Author:

Tuomas Aalto

Supervisor:

Sami Nurmi

JYVÄSKYLÄN YLIOPISTO
UNIVERSITY OF JYVÄSKYLÄ

Abstract

Aalto, Tuomas
The First-Order Evolution of Cosmic Scalar Perturbations
Master's thesis
Department of Physics, University of Jyväskylä, 2019, 89 pages.

According to the current understanding, the early universe was close to homogeneity with small perturbations left as remnants of the inflation. How these small perturbations evolved into the cosmic structures we observe today is one of the central topics in cosmology.

Of different types of perturbations, it is the scalar ones that most dominantly couple to perturbations in energy density and lead to structure formation. This thesis is a review of the well-established evolution of the cosmic scalar perturbations within the context of linear cosmological perturbation theory. We present the derivation of the equations governing the evolution of the scalar perturbations starting from the cosmological perturbation theory. The derivation is done in the Newtonian gauge.

Rudimentary solutions to the evolution equations are also presented, both through analytical approximations and numerical computations. In the emerging picture, the structure formation starts with the accumulation of dark matter in radiation dominance. Baryonic matter is prevented from accumulation until decoupling from the photons at the redshift $z \approx 1000$.

The validity of the perturbative method is examined through a comparison with the spherical collapse model of structure formation. This well known comparison shows how the linear perturbation theory underestimates the growth of perturbations in the energy density.

Keywords: cosmology, large scale structure, structure formation, cosmological perturbation theory

Tiivistelmä

Aalto, Tuomas
Kosmisten skalaarihäiriöiden ensimmäisen asteen kehitys
Pro gradu -tutkielma
Fysiikan laitos, Jyväskylän yliopisto, 2019, 89 sivua

Nykytietämyksen mukaan kosminen inflaatio jätti pieniä häiriöitä lähes homogeeniseen varhaiseen maailmankaikkeuteen. Nykyään havaittavien kosmisten rakenteiden kehittyminen näistä häiriöistä on yksi kosmologian keskeisistä osa-alueista.

Rakenteiden muodostumisen kannalta keskeisimpiä ovat skalaarityyppiset häiriöt, joihin maailmankaikkeuden energiatiheyden häiriöt pääasiallisesti kytkeytyvät. Tämä tutkielma on katsaus lineaarisen kosmologisen häiriöteorian antamaan hyvin tunnettuun kuvaukseen skalaarihäiriöiden kehittymiselle. Skalaarihäiriöiden kehittymistä kuvaavien yhtälöiden johto esitetään kosmologisesta häiriöteoriasta alkaen. Yhtälöt on johdettu newtonilaista mittaa käyttäen.

Häiriöiden kehitystä kuvaaville yhtälöille esitetään sekä analyyttisillä approksimaatioilla että numeerisella laskennalla saatavia viitteellisiä ratkaisuja. Muodostuvassa mallissa rakenteiden syntyminen alkaa pimeän aineen kasautumisella säteilyn dominanssin aikana. Baryonisen aineen kasautuminen pääsee alkamaan vasta sen irtikytkeydyttyä fotoneista punasiirtymän $z \approx 1000$ kohdalla.

Häiriöteoriaan perustuvan menetelmän validisuutta tarkastellaan vertaamalla saatuja tuloksia rakenteenmuodostumisen pallomaisen romahdusmallin kanssa. Tämä entuudestaan tunnettu vertailu näyttää, kuinka lineaarinen häiriöteoria aliarvioi energiatiheyden häiriöiden kasvua.

Avainsanat: kosmologia, suuren skaalan rakenne, rakenteen muodostuminen, lineaarinen perturbaatioteoria

Contents

1 Introduction

In the universe we observe today, the structures on supergalactic scales form a hierarchical system from groups and clusters of galaxies to superclusters, walls and filaments [1, 2]. This Large Scale Structure (LSS) has evolved from small perturbations in the nearly homogeneous early universe. Detailed understanding of the highly non-linear structure formation process is one of the major challenges in modern cosmology.

At the theoretical heart of cosmology is the general relativity. General relativity is a theory of gravity in which gravity is attributed to the curvature of spacetime. General relativity describes the dynamics of the universe: how energy and momentum affect the spacetime and vice versa.

In the basic model of the universe used in cosmology, the Friedmann-Robertson-Walker (FRW) universe, the universe is assumed to be spatially homogeneous and isotropic. The FRW universe describes the average dynamics on scales larger than 100 Mpc. The requirements of homogeneity and isotropy must be relieved when modelling a universe with structures. In cosmological perturbation theory, the structures are described by a layer of perturbations added onto the FRW universe [3–5]. Cosmological perturbation theory sets the theoretical framework of early structure formation analysis.

The evolution of the cosmological perturbations can be traced with the cosmological perturbation theory. From the perspective of structure formation, the quantity of most interest is the perturbation in energy density, especially that of matter. By definition, the perturbation in matter energy density is the deviation of energy density of matter from its homogeneous, FRW universe value. As such, it measures the accumulation of matter under gravity to form structures.

Solving the evolution of matter perturbations in detail requires solving the evolution of perturbations of other components of the cosmic plasma as well. This is due to both direct interactions between the components and indirect interactions through the metric [6, 7]. However, in linear cosmological perturbation theory, where perturbations are dealt with only up to the first order, one is able to restrict the analysis to a category of perturbations known as the scalar perturbations [3]. Invoking a higher order perturbation theory increases the complexity of the analysis significantly [8, 9] while still being limited by the requirement of small perturbations. Matter accumulating to form structures on a given scale eventually causes the perturbations to reach a point where a perturbation theory of any order is rendered invalid on that scale.

A simple and well-known method for estimating the validity of the structure formation analysis based on cosmological perturbation theory is comparing its results with those of the spherical collapse model [10]. In the spherical collapse model,

a collapsing structure is a closed FRW universe of its own, embedded in a flat FRW background universe. The model is a quite limited representation of the collapsing process, but it reveals some shortcomings of the results given by linear perturbation theory. The region of structure formation where the perturbative method is unapplicable can be studied with N-body simulations [11–13].

For cosmological perturbation theory to be able to trace the evolution of perturbations, the initial state of the perturbations must be established. The birth of cosmological perturbations is most likely explained by inflation [14–16]. Inflation is a period during which the expansion of the universe is accelerated under the supposed influence of an inflaton field. Inflation precedes the radiation dominated epoch of the universe. Fluctuations of the inflaton field persist as the seeds of structure formation [17]. Notably, the perturbations produced by the inflation are predicted to be nearly scale-invariant and adiabatic [17], in agreement with observations [18].

The first few sections of this thesis introduce the preliminaries required by the derivation of the perturbation equations. Section 2 briefly covers the main concepts of general relativity. In section 3, the tools of GR are applied to a homogeneous and isotropic metric, resulting in FRW cosmology. In section 4, a perturbation is added to the FRW universe, leading to the cosmological perturbation theory.

At the core of this thesis is the derivation of equations governing the evolution of different components of the cosmic fluid within the context of linear cosmological perturbation theory in section 5. The section 5 also establishes the initial conditions for the derived differential equations. Rudimentary solutions to the derived equations are given in section 6, both through analytic approximations and numerical computations. The validity of the analysis is assessed in section 7 by a comparison with the spherical collapse model.

This thesis is review-like in nature, with all of the presented concepts and methods previously established in literature.

1.1 Notation and Conventions

The natural units used throughout this thesis are defined by setting

$$c \equiv \hbar \equiv k_{\mathrm{B}} \equiv 1. \tag{1}$$

In indices, greek alphabets run from 0 to 3 and latin alphabets from 1 to 3. The Einstein summation convention is used, so that summation is implied over an index appearing both in subscript and superscript positions:

$$q^{\mu} q_{\mu} \equiv \sum_{\mu=0}^{3} q^{\mu} q_{\mu}. \tag{2}$$

The present day value of quantity q is denoted with a subscript zero as q_0.

2 General Relativity in Brief

General relativity is a theory of space, time and gravity. In general relativity, gravity is a manifestation of the curvature of spacetime. Gravitational interactions occur through the spacetime: mass curves the spacetime and the curvature of spacetime affects the trajectories of particles. The tight constraints on the theory of gravity from observations on a wide range of distance and mass scales agree extremely well with general relativity (see e.g. [19, 20]).

In this short overview of general relativity, two key components of the theory are introduced. The first one is the set of Einstein field equations, which describes how spacetime is curved by energy and momentum. The second component is the geodesic equation, which governs the motion of free particles in curved spacetime. There will be little in the way of derivation for these results in this section or inspection of the mathematical basis of general relativity. For a detailed introduction to general relativity, see for example [21].

2.1 The Einstein Equations

The concept of spacetime appears already in special relativity where gravity is not present. Unlike in Newtonian mechanics where there is a universal notion of time, in special relativity the time span between two events depends on reference frame. A meaningful measure for distance between two events is given by the spacetime interval

$$\begin{aligned} \Delta s^2 &\equiv -\Delta t^2 + \Delta x^2 + \Delta y^2 + \Delta z^2 \\ &= \eta_{\mu\nu} \Delta x^\mu \Delta x^\nu. \end{aligned} \tag{3}$$

In (3), $\eta_{\mu\nu}$ is the Minkowski metric,

$$\eta_{\mu\nu} = \mathrm{Diag}(-1, 1, 1, 1). \tag{4}$$

The spacetime of special relativity has a simple, flat geometry, described by the Minkowski metric (4).

General relativity is a more general theory than special relativity because it includes gravity. Taking the spacetime interval Δs^2 to the infinitesimal limit, a line element is introduced as

$$ds^2 = g_{\mu\nu} dx^\mu dx^\nu \tag{5}$$

with a general metric $g_{\mu\nu}$. With the line element the distance between two spacetime points can be defined on a curve connecting the points.

The metric $g_{\mu\nu}$ specifies the geometry of the spacetime. In general relativity, this geometry is identified as gravity when $g_{\mu\nu} \neq \eta_{\mu\nu}$. The gravitation law of general

relativity describes how the geometry, or the metric, depends on the distribution of energy and momentum in the universe. The law is given by the Einstein equations (see e.g. [21]):

$$G_{\mu\nu} = M_{\mathrm{p}}^{-2} T_{\mu\nu}. \tag{6}$$

The Einstein tensor $G_{\mu\nu}$ is directly determined by the metric, as will be shown briefly. The energy-momentum tensor $T_{\mu\nu}$ describes the energy and momentum related properties of the system: energy density, pressure, stress and so on. The coupling constant M_{P} is the reduced Planck mass, relating to the Newton's gravitation constant by $M_{\mathrm{P}}^{-2} = 8\pi G_{\mathrm{N}}$. In the limit of weak gravity, the metric is

$$g_{\mu\nu} = \eta_{\mu\nu} + \delta g_{\mu\nu}, \qquad |\delta g_{\mu\nu}| \ll 1. \tag{7}$$

At this limit, the Einstein equations (6) reduce to the Newton's gravitation law

$$\nabla^2 \Phi = 4\pi G_{\mathrm{N}} \rho. \tag{8}$$

As will be discussed next, the Einstein tensor contains second derivatives of the metric, so the metric generalizes the gravitation potential Φ of Newton's gravitation law, and the energy-momentum tensor generalizes the mass distribution ρ.

The curvature of the spacetime is characterized by the Riemann curvature tensor (see e.g. [21])

$$R^{\rho}{}_{\sigma\mu\nu} = \partial_\mu \Gamma^{\rho}_{\nu\sigma} - \partial_\nu \Gamma^{\rho}_{\mu\sigma} + \Gamma^{\rho}_{\mu\lambda}\Gamma^{\lambda}_{\nu\sigma} - \Gamma^{\rho}_{\nu\lambda}\Gamma^{\lambda}_{\mu\sigma}, \tag{9}$$

where $\Gamma^{\sigma}_{\mu\nu}$ is the Christoffel symbol

$$\Gamma^{\sigma}_{\mu\nu} = \frac{1}{2} g^{\sigma\rho}(\partial_\mu g_{\nu\rho} + \partial_\nu g_{\rho\mu} - \partial_\rho g_{\mu\nu}). \tag{10}$$

The Ricci tensor is defined as a contraction of the Riemann curvature tensor:

$$R_{\mu\nu} \equiv R^{\lambda}{}_{\mu\lambda\nu}. \tag{11}$$

The trace of the Ricci tensor is known as the Ricci scalar

$$R \equiv R^{\lambda}{}_{\lambda}. \tag{12}$$

The Einstein tensor is then defined with Ricci tensor and scalar as (see e.g. [21])

$$G_{\mu\nu} \equiv R_{\mu\nu} - \frac{1}{2} R g_{\mu\nu}. \tag{13}$$

From the equations (9) and (10) we see that the elements of the Riemann tensor are composed from second derivatives of the metric. Since the Einstein tensor $G_{\mu\nu}$ is built of contractions of the Riemann tensor, it too is composed of second derivatives of the metric.

Because the Ricci tensor is a contraction of the Riemann curvature tensor, it does not contain all the degrees of freedom of the Riemann curvature tensor. The Ricci tensor characterizes curvature from local energy-momentum properties as per the

Einstein equations (6). The remaining degrees of freedom in the Riemann curvature tensor describe curvature from non-local sources, corresponding to gravitational waves (see e.g. [21]).

The form of the energy-momentum tensor of most practical use is that of a perfect fluid:

$$T_{\mu\nu} = (\rho + p)u_\mu u_\nu + p g_{\mu\nu}, \tag{14}$$

with ρ being the energy density of the fluid, p its pressure and u^μ its four-velocity. Deviations from the perfect fluid form introduce an anisotropic stress tensor $\Pi_{\mu\nu}$. The energy-momentum tensor then becomes

$$T_{\mu\nu} = (\rho + p)u_\mu u_\nu + p\left(g_{\mu\nu} + \Pi_{\mu\nu}\right). \tag{15}$$

The anisotropic stress tensor is symmetric and traceless with $\Pi^\mu{}_0 = \Pi^0{}_\mu = 0$.

In general, the partial derivative of a vector $\partial_\mu V^\nu$ is not a tensor. The derivation operation that transforms as a tensor is the covariant derivative, constructed with the Christoffel symbol:

$$\nabla_\mu V^\nu = \partial_\mu V^\nu + \Gamma^\nu_{\mu\lambda} V^\lambda. \tag{16}$$

Similarly for duals

$$\nabla_\mu \omega_\nu = \partial_\mu \omega_\nu - \Gamma^\lambda_{\mu\nu} \omega_\lambda. \tag{17}$$

The covariant derivative generalizes to higher rank tensors in a simple manner, containing a term with the Christoffel symbol for every index.

From the symmetries of the Riemann curvature tensor $R^\rho{}_{\sigma\mu\nu}$ it follows that the contraction of the Einstein tensor with the covariant derivative vanishes:

$$\nabla_\mu G^\mu{}_\nu = 0. \tag{18}$$

Together with the Einstein equations (6) this implies a similar equation for the energy-momentum tensor:

$$\nabla_\mu T^\mu{}_\nu = 0. \tag{19}$$

The equation (19) is the continuity law of energy and momentum in general relativity.

2.2 The Geodesic Equation

Energy and momentum determine the geometry of spacetime according to the Einstein equations (6). Trajectories of free particles subject only to gravity are given by the geodesic equation

$$\frac{dx^\nu}{d\lambda} \nabla_\nu \frac{dx^\mu}{d\lambda} = 0. \tag{20}$$

The solutions to the geodesic equation are curves $x^\mu(\lambda)$ in the spacetime, λ being the curve parameter. The geodesic equation plays a similar role in general relativity as the Newton's second law $\mathbf{F} = m\mathbf{a}$ in Newtonian mechanics for a particle subject to the gravitational force $\mathbf{F}$.

For massive particles, the proper time τ is a natural choice for the curve parameter λ. With the four-momentum $p^\mu = m\,dx^\mu/d\tau$ the geodesic equation (20) is then equivalent with

$$p^\nu \nabla_\nu p^\mu = 0. \tag{21}$$

For massless particles, the curve parameter λ can be chosen so that $p^\mu = dx^\mu/d\lambda$. Therefore the equation (21) holds also for massless particles. With the equations (16) and (21), the geodesic equation can be written as

$$m\frac{dp^\mu}{d\tau} + \Gamma^\mu_{\rho\sigma} p^\rho p^\sigma = 0 \tag{22}$$

for massive particles and

$$\frac{dp^\mu}{d\lambda} + \Gamma^\mu_{\rho\sigma} p^\rho p^\sigma = 0 \tag{23}$$

for massless particles.

3 FRW Cosmology

With the machinery of general relativity set up in section 2, we are ready to solve the Einstein equations (6) in the physical situation most interesting to cosmology: the homogeneous and isotropic universe. This system, where energy is evenly distributed and no direction is special, provides a reasonable description of our universe on scales larger than 100 Mpc [22, 23]. It also goes by the name of Friedmann-Robertson-Walker (FRW) universe after the pioneers of the model. In cosmological perturbation theory, which is the subject of section 4, the FRW universe is the background solution on top of which the perturbation is added.

3.1 The Robertson-Walker Metric

The most general metric describing a homogeneous and isotropic spacetime is the Robertson-Walker metric, which in polar coordinates has the form (see e.g. [21])

$$ds^2 = -dt^2 + a^2(t)\left(\frac{dr^2}{1-Kr^2} + r^2 d\theta^2 + r^2 \sin^2\theta\, d\phi^2\right). \tag{24}$$

The scale factor $a(t)$ is the sole dynamical variable of the RW metric. The constant parameter K relates to spatial curvature. In a spatially flat spacetime $K = 0$.

Observations are consistent with the observable universe having no significant spatial curvature [18]. It is therefore often justified to ignore the curvature parameter K in (24). The RW metric in Cartesian coordinates is then

$$ds^2 = -dt^2 + a^2(t)\left(dx^2 + dy^2 + dz^2\right). \tag{25}$$

Spatial curvature becomes relevant when discussing the spherical collapse model in section 7.

Homogeneity and isotropy force the energy-momentum tensor to be of the perfect fluid form (14). The cosmic fluid is at rest with respect to the comoving coordinate system, so its four-velocity is $u^\mu = (1, 0, 0, 0)$. Computing the Einstein tensor from the metric (24) with equations (9) – (13) and applying the Einstein equations (6) results in (see e.g. [21])

$$\left(\frac{\dot{a}}{a}\right)^2 = \frac{\rho}{3M_{\mathrm{P}}^2} - \frac{K}{a^2} \tag{26}$$

$$\frac{\ddot{a}}{a} = -\frac{\rho + 3p}{6M_{\mathrm{P}}^2}. \tag{27}$$

Here the dots denote time derivatives. The equations (26) and (27) are known as the Friedmann equations, with *the* Friedmann equation referring to (26). The logarithmic rate of change of the scale factor a is known as the Hubble parameter,

$$H \equiv \frac{d \ln a}{dt} = \frac{\dot{a}}{a}. \tag{28}$$

The scaling of the scale factor is in principle arbitrary, but its relative changes are observable as the redshift z:

$$\frac{a_0}{a(t)} = 1 + z(t). \tag{29}$$

The quantity z is known as the redshift because the wavelength of a photon emitted at time t and detected at present time t_0 has by the time of detection increased by factor $1 + z(t)$ due to expansion of space (see e.g. [21]).

3.2 Fluid Components

The Friedmann equations (26) and (27) determine how the evolution of the scale factor a depends on the properties of the cosmic fluid, namely its energy density ρ and pressure p. The properties of the fluid in turn depend on its composition and the properties of the components.

The equation of state $p_i = p_i(\rho_i)$ of a fluid component i expresses the dependence of pressure on energy density. In the perfect fluid model the components of the cosmic fluid have a particularly simple equation of state with a constant equation of state parameter w_i:

$$p_i = w_i \rho_i. \tag{30}$$

For the whole fluid the equation of state parameter w is defined similarly as

$$w \equiv \frac{p}{\rho}, \tag{31}$$

where $p = \sum p_i$ and $\rho = \sum \rho_i$. In general, the parameter w varies with time even if w_i is a constant for all of the fluid components.

A fluid component is unrelativistic if its temperature is well below particle mass. This is what we label as matter. Pressure of matter is negligible, so that its equation of state parameter is $w_\mathrm{m} = 0$. Radiation consists of relativistic particles. The equation of state for radiation is $w_\mathrm{r} = 1/3$. In the concordance model of cosmology, the ΛCDM model, there is a third kind of fluid component: the vacuum energy (see e.g. [24]). In ΛCDM, the current acceleration of expansion of space is due to vacuum energy. Vacuum energy has equation of state parameter $w_\Lambda = -1$.

In the FRW universe, the continuity of energy and momentum (19) has the form

$$\dot{\rho} = -3H(\rho + p), \tag{32}$$

which holds both for the fluid as a whole and for its individual components. For a fluid component i with a constant equation of state parameter w_i the continuity (32) implies the dependence of energy density ρ_i on scale factor a:

$$\rho_i \propto a^{-3(1+w_i)}. \tag{33}$$

Hence the energy densities of matter, radiation and vacuum energy evolve as

$$\rho_{\mathrm{m}} \propto a^{-3} \tag{34}$$

$$\rho_{\mathrm{r}} \propto a^{-4} \tag{35}$$

$$\rho_\Lambda = \text{const}, \tag{36}$$

respectively.

The energy density of fluid component i is often expressed through its density parameter

$$\Omega_i \equiv \frac{\rho_i}{\rho_{\mathrm{c}}}, \tag{37}$$

where ρ_{c} is the critical density

$$\rho_{\mathrm{c}} \equiv 3M_{\mathrm{P}}^2 H^2. \tag{38}$$

From the Friedmann equation (26) we see that the curvature parameter K vanishes when the energy density of the whole fluid is equal to the critical density ρ_{c}. Setting the density parameter of the whole fluid $\Omega \equiv \rho/\rho_{\mathrm{c}}$ to unity, we get from the Friedmann equation (26)

$$H^2 = H_0^2 \left(\Omega_{\mathrm{r}0} \left(\frac{a_0}{a} \right)^4 + \Omega_{\mathrm{m}0} \left(\frac{a_0}{a} \right)^3 + \Omega_{\Lambda 0} \right). \tag{39}$$

From the scale factor dependence of different fluid components (34) – (36) we see how the history of the universe divides into epochs during which the energy density of one of the components dominates over all the others. Here we are setting aside the period of inflation which precedes all the discussed epochs. Going back in time the scale factor approaches zero. With the radiation density $\rho_{\mathrm{r}} \propto a^{-4}$ growing faster than that of matter $\rho_{\mathrm{m}} \propto a^{-3}$ or vacuum energy $\rho_\Lambda = \text{const}$ when $a \to 0$, the first epoch is radiation dominated. Using (29) and (37) with (34) and (35), the redshift z_{eq} at which energy densities of radiation and matter are equal is

$$z_{\mathrm{eq}} = \frac{\Omega_{\mathrm{m}0}}{\Omega_{\mathrm{r}0}} - 1. \tag{40}$$

With the measured parameter values [18] listed in appendix A, $z_{\mathrm{eq}} \approx 3400$. At that point, the universe enters the matter dominated epoch. Similarly with the energy density of matter and vacuum energy evolving as (34) and (36), respectively, the universe enters the vacuum energy dominated epoch at [18]

$$\begin{aligned} z &= \left(\frac{\Omega_{\Lambda 0}}{\Omega_{\mathrm{m}0}} \right)^{1/3} - 1 \\ &\approx 0.31. \end{aligned} \tag{41}$$

3.3 Conformal Time

The so called conformal time η is defined as

$$dt \equiv a\, d\eta. \tag{42}$$

Conformal time is often a convenient choice of time coordinate when spatial curvature is negligible. With the conformal time, the spatially flat RW metric (25) becomes

$$g_{\mu\nu} = a^2(\eta)\eta_{\mu\nu}, \tag{43}$$

where $\eta_{\mu\nu}$ is the Minkowski metric (4).

The comoving Hubble parameter $\mathcal{H}$ is defined by

$$\mathcal{H} \equiv \frac{d\ln a}{d\eta} = \frac{a'}{a} = \dot{a} = aH, \tag{44}$$

where the derivative with respect to conformal time is denoted by prime: $(\ )' \equiv d/d\eta$. Using the conformal time, the Friedmann equations (26) and (27) with $K = 0$ become

$$\mathcal{H}^2 = \frac{\rho a^2}{3M_{\rm p}^2} \tag{45}$$

$$\mathcal{H}' = -\frac{(\rho + 3p)a^2}{6M_{\rm p}^2}. \tag{46}$$

4 Cosmological Perturbation Theory

The FRW universe sets a solid foundation for cosmology [22, 23], but approximating the universe to be homogeneous and isotropic is applicable only up to a point. A universe in which matter accumulates to form structure is not a homogeneous one.

Structure formation can be approached perturbatively. In cosmological perturbation theory, the FRW universe is taken as a background, and a layer of perturbations is added on top of it. As with the FRW universe, the perturbed universe is characterized by its metric. The perturbed metric is of the form

$$g_{\mu\nu} = \bar{g}_{\mu\nu} + \delta g_{\mu\nu} \tag{47}$$

with the background part $\bar{g}_{\mu\nu}$ being the Robertson-Walker metric of (25) and $\delta g_{\mu\nu}$ a small perturbation.

The perturbation $\delta g_{\mu\nu}$ is assumed to be small in comparison to the background value $\bar{g}_{\mu\nu}$ so that terms higher order in $\delta g_{\mu\nu}$ can be ignored. The simplest choice, applied throughout this thesis, is to keep terms only up to first order in $\delta g_{\mu\nu}$, resulting in linear perturbation theory. Going up to second order in perturbations increases the complexity of the theory significantly [8, 9].

When dividing the metric $g_{\mu\nu}$ into background part $\bar{g}_{\mu\nu}$ and perturbation $\delta g_{\mu\nu}$ a choice is made, since the division is not unique. This freedom of choice acts as a gauge freedom of the theory, with a particular choice of division fixing the gauge. Until the gauge is fixed, there are non-physical degrees of freedom, or gauge modes, in the theory. (See e.g. [5].)

Different gauges have been used within the context of cosmological perturbation theory with certain gauges usually being better suited for some situations than others. Especially before the 1980s, what is known as the synchronous gauge was the most common one, used for example in the influential textbook by Peebles [25]. The synchronous gauge, however, has the inconvenient property of not being fully fixed, leading to difficulty in interpretation of the physical implications of the theory. One solution, presented by Bardeen [26], is to write the theory in terms of gauge invariant variables, which are unaffected by gauge modes. An approach combining the physical clarity of a gauge invariant theory and computational simplicity of a fixed-gauge theory is to fix the gauge in such a way that the remaining variables are gauge invariant. This is the approach adopted in this thesis, where we shall be using the Newtonian gauge. In the Newtonian gauge, the perturbation of the metric $\delta g_{\mu\nu}$ is written in terms of the gauge invariant variables introduced by Bardeen. (See e.g. [5].)

The goal of this section is to lay a solid foundation for the perturbed universe whose dynamics will be solved in upcoming sections. Some amount of technical details are presented here to establish the physical and mathematical considerations

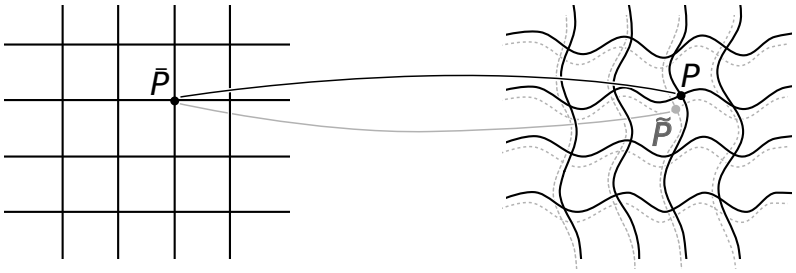

Figure 1. With a perturbed spacetime built on top of the FRW spacetime, a point $\bar{P}$ in the FRW universe is associated with a point P in the perturbed universe. In a different gauge the point $\bar{P}$ is associated with a different point $\tilde{P}$.

required by the perturbed universe. For a more complete discussion on cosmological perturbation theory, see e.g. [4, 5]. From practical point of view, however, there are essentially only two key results that make reappearences in following sections: vector and tensor perturbations can be ignored while discussing structure formation, and the perturbed metric has the form (91).

While improving the cosmological description of the universe over the FRW model, a perturbation theory with perturbations up to any order has a limited scope. That is because at some point in the structure formation the accumulation of matter reaches a point when perturbations are no longer small in comparison to the background. To study structure formation beyond that point, N-body simulations are used, as in [11–13]. The point at which the perturbative approach breaks depends on at what scale the universe is inspected: the larger the scale, the smoother the universe. To examine the perturbations on different scales, much of the analysis of cosmological perturbations is done in the Fourier space, discussed in section 4.3.

4.1 Gauge Transformations

To build a perturbed universe by adding a perturbation to the FRW universe we need a one-to-one correspondence between the spacetime points of the two universes. As a manifestation of the gauge freedom, there is no unique choice of mapping between the spacetimes: a given point in the background spacetime can be associated with several points close to each other in the perturbed universe. The situation is illustrated in figure 1.

The mapping between the background and the perturbed spacetime is established through coordinate systems. Let $\{\bar{x}^\mu\}$ be the coordinate system in the background spacetime and $\{x^\mu\}$ and $\{\tilde{x}^\mu\}$ the coordinate systems associating the background point $\bar{P}$ with perturbed spacetime points P and $\tilde{P}$ respectively. The coordinate systems are related by

$$\bar{x}^\mu(\bar{P}) = x^\mu(P) = \tilde{x}^\mu(\tilde{P}). \tag{48}$$

Let us denote the difference between coordinates of a single point by ξ^μ, so that

$$\tilde{x}^\mu(P) = x^\mu(P) + \xi^\mu(P) \tag{49}$$
$$\tilde{x}^\mu(\tilde{P}) = x^\mu(\tilde{P}) + \xi^\mu(\tilde{P}). \tag{50}$$

The equations (49) and (50) establish the gauge transformations between the two gauges. The difference of differences $\xi^\mu(P) - \xi^\mu(\tilde{P})$ is second order in perturbation and thus can be ignored:

$$\xi^\mu(P) = \xi^\mu(\tilde{P}) \equiv \xi^\mu. \tag{51}$$

A scalar quantity q by definition is unchanged by a coordinate transformation. The background and perturbation parts $\bar{q}$ and δq, however, do change under coordinate transformations, as they are not tensoral. This reflects the fact that they are not directly observables like q. Next we shall determine the effect a coordinate transformation of the form (49) has on the perturbative part δq. This is a stepladder towards the transformation of the quantity of most interest to us, the metric.

By definition the perturbation is the difference between the total value and the background value. In the two different gauges then

$$\delta q(\bar{P}) = q(P) - \bar{q}(\bar{P}) \tag{52}$$
$$\widetilde{\delta q}(\bar{P}) = q(\tilde{P}) - \bar{q}(\bar{P}). \tag{53}$$

Note that both the background value $\bar{q}$ and the perturbation δq are functions of the background spacetime, since the value of both of them in a single point in the perturbed spacetime depends on the chosen gauge. The total quantity q at point $\tilde{P}$ can be approximated with an expansion around point P:

$$q(\tilde{P}) = q(P) + \partial_\mu q(P) \left(x^\mu(\tilde{P}) - x^\mu(P) \right). \tag{54}$$

With different coordinates relating through (48) and (50), the equation (54) yields

$$\widetilde{\delta q}(\bar{P}) = \delta q(\bar{P}) - \xi^\mu \partial_\mu q(P). \tag{55}$$

Dropping second order terms gives the gauge transformation law for the perturbation of a scalar quantity:

$$\widetilde{\delta q}(\bar{P}) = \delta q(\bar{P}) - \xi^0 \bar{q}'(\bar{P}). \tag{56}$$

Unlike scalars, the components of a type (0,2) tensor $B_{\mu\nu}$ are not unchanged under a coordinate tranformation but tranformed as

$$B_{\tilde{\mu}\tilde{\nu}} = \frac{\partial x^\alpha}{\partial \tilde{x}^{\tilde{\mu}}} \frac{\partial x^\beta}{\partial \tilde{x}^{\tilde{\nu}}} B_{\alpha\beta}. \tag{57}$$

The gauge transformation (49) implies

$$\frac{\partial x^\mu}{\partial \tilde{x}^{\tilde{\nu}}} = \delta^\mu_{\tilde{\nu}} - \partial_{\tilde{\nu}} \xi^\mu. \tag{58}$$

As with the scalar field, expressing the tensor $B_{\mu\nu}$ at point $\tilde{P}$ in terms of expansion around P gives

$$B_{\mu\nu}(\tilde{P}) = B_{\mu\nu}(P) - \xi^0 \bar{B}'_{\mu\nu}(\bar{P}). \tag{59}$$

Using the coordinate transformation law (57):

$$B_{\tilde{\mu}\tilde{\nu}}(\tilde{P}) = \frac{\partial x^\alpha}{\partial \tilde{x}^{\tilde{\mu}}} \frac{\partial x^\beta}{\partial \tilde{x}^{\tilde{\nu}}} \left(B_{\alpha\beta}(P) - \xi^0 \bar{B}'_{\alpha\beta}(\bar{P}) \right). \tag{60}$$

Applying (58) and dropping higher order terms results in the gauge transformation law

$$\widetilde{\delta B_{\mu\nu}} = \delta B_{\mu\nu} - \xi^0 \bar{B}'_{\mu\nu} - \bar{B}_{\mu\lambda}\partial_\nu \xi^\lambda - \bar{B}_{\lambda\nu}\partial_\mu \xi^\lambda. \tag{61}$$

Transformations for different types of tensors can be derived similarly, but the transformation law of (61) will be the one needed when deriving the form of the perturbed metric in the next section.

4.2 The Perturbed Metric

Solving the dynamics of the perturbed universe proceeds in the manner seen with the FRW universe in section 3: we specify the metric from geometric properties and the energy-momentum tensor from physical properties and use the Einstein equations (6). Most focus will be on the metric, as it is with the metric that we shall fix the gauge. This gauge choice will then propagate to the energy-momentum tensor through the Einstein equations in section 5.2.

To start deriving the perturbed metric, let us label the components of its perturbation $\delta g_{\mu\nu}$:

$$\delta g_{\mu\nu} = a^2(\eta) \begin{pmatrix} -2A & -B_i \\ -B_i & -2D\delta_{ij} + 2E_{ij} \end{pmatrix}. \tag{62}$$

In (62), the matrix E_{ij} is traceless

$$\delta^{ij} E_{ij} = 0, \tag{63}$$

making the division between E_{ij} and $D\delta_{ij}$ unique. The D component then relates to the trace of δg_{ij} by

$$D = -\frac{1}{6a^2} \delta^{ij} \delta g_{ij}. \tag{64}$$

With (62), the ten parameters of $\delta g_{\mu\nu}$ are labelled by A, B_i, D and E_{ij}, the last being a symmetric and traceless matrix. However, not all of these degrees of freedom are relevant for structure formation. To separate the relevant components from the rest, we shall perform a scalar-vector-tensor (SVT) decomposition (see e.g. [27]). The decomposition separates components based on their behaviour under global rotations of the background spacetime. While $\delta g_{\mu\nu}$ or its components do not transform as tensors under a general coordinate transformations, limiting to rotations sees the components transform in a tensorial fashion. In the end, it will be the components behaving like scalars that we will be interested in.

A general spatial rotation

$$R^{\mu}{}_{\nu} = \begin{pmatrix} 1 & 0 \\ 0 & R^{i}{}_{j} \end{pmatrix} \tag{65}$$

has the defining properties $R^{i}{}_{k}R_{j}{}^{k} = \delta^{i}_{j}$ and $\det(R) = 1$. Rotating the total metric

$$g_{\tilde{\mu}\tilde{\nu}} = R^{\alpha}{}_{\tilde{\mu}}R^{\beta}{}_{\tilde{\nu}}g_{\alpha\beta} \tag{66}$$

with perturbation components labelled as in (62) results in transformations

$$\tilde{A} = A \tag{67}$$

$$\tilde{D} = D \tag{68}$$

$$B_{\tilde{i}} = R^{j}{}_{\tilde{i}}B_{j} \tag{69}$$

$$E_{\tilde{i}\tilde{j}} = R^{k}{}_{\tilde{i}}R^{l}{}_{\tilde{j}}E_{kl}. \tag{70}$$

Hence A and D are scalars, B_i a 3-vector and E_{ij} a (0,2)-tensor under global rotations of the background spacetime.

An additional scalar field can be extracted from B_i. Consider the Helmholtz decomposition of the vector field B_i

$$B_i = B_i^{\mathrm{S}} + B_i^{\mathrm{V}}, \tag{71}$$

with the vector field B_i^{S} having zero curl and B_i^{V} being divergenceless. The curl-free B_i^{S} can be expressed as the gradient of a scalar field B

$$B_i^{\mathrm{S}} \equiv \partial_i B, \tag{72}$$

defining the field B.

A similar treatment of the tensor field E_{ij} breaks it into three parts (see e.g. [27])

$$E_{ij} = E_{ij}^{\mathrm{S}} + E_{ij}^{\mathrm{V}} + E_{ij}^{\mathrm{T}}. \tag{73}$$

In (73), E_{ij}^{S} defines a scalar field E:

$$E_{ij}^{\mathrm{S}} \equiv (\partial_i\partial_j - \frac{1}{3}\delta_{ij}\nabla^2)E. \tag{74}$$

A divergenceless vector field E_i can be extracted from E_{ij}^{V}:

$$E_{ij}^{\mathrm{V}} \equiv \frac{1}{2}(\partial_j E_i + \partial_i E_j). \tag{75}$$

The remaining component E_{ij}^{T} constitutes a transverse and traceless tensor:

$$\delta^{ij}E_{ij}^{\mathrm{T}} = 0 \tag{76}$$

$$\delta^{ik}\partial_k E_{ij}^{\mathrm{T}} = 0. \tag{77}$$

The perturbation degrees of freedom in the metric $g_{\mu\nu}$ are now categorized by four scalar perturbations A, B, D and E, divergenceless vector fields B_i and E_i and a transverse and traceless tensor field E_{ij}^{T}. The scalar perturbations are the most relevant ones from the point of view of the structure formation since they couple to perturbations in energy density and pressure. The vector perturbations decay and hence have little relevance [3]. The tensor perturbations describe gravitational waves.

Up to linear order in perturbations, the different categories of perturbations develop independent of each other (see e.g. [4]). The formation of structure is reflected in the perturbation of energy density, $\delta\rho$. Because $\delta\rho$ is a scalar, we are able to ignore all but the scalar perturbations while analyzing the structure formation within the context of linear perturbation theory. Without the vector and tensor perturbations the perturbation of the metric has the form

$$\delta g_{\mu\nu} = a^2(\eta) \begin{pmatrix} -2A & -\partial_i B \\ -\partial_i B & -2D\delta_{ij} + 2(\partial_i\partial_j - \frac{1}{3}\delta_{ij}\nabla^2)E \end{pmatrix}. \tag{78}$$

Up to this point no gauge has been specified. As it turns out, two of the degrees of freedom in (78) are gauge modes. Fixing the gauge in a suitable manner is the last step in specifying the perturbed metric.

Transforming the perturbation of the metric (78) with (61), we see that the scalar perturbations change under a gauge transformation (49) as

$$\tilde{A} = A - \mathcal{H}\xi^0 - \xi^{0\prime}, \tag{79}$$

$$\partial_i\tilde{B} = \partial_i B + \xi^{i\prime} - \partial_i\xi^0, \tag{80}$$

and

$$\begin{aligned} &\tilde{D}\delta_{ij} - (\partial_i\partial_j - \frac{1}{3}\delta_{ij}\nabla^2)\tilde{E} = \\ &\quad D\delta_{ij} - (\partial_i\partial_j - \frac{1}{3}\delta_{ij}\nabla^2)E + \mathcal{H}\xi^0\delta_{ij} + \frac{1}{2}(\partial_i\xi^j + \partial_j\xi^i). \end{aligned} \tag{81}$$

Separating (81) into trace and a traceless part gives separate eqations for D and E:

$$\tilde{D} = D + \mathcal{H}\xi^0 + \frac{1}{3}\partial_k\xi^k \tag{82}$$

and

$$\begin{aligned} &(\partial_i\partial_j - \frac{1}{3}\delta_{ij}\nabla^2)\tilde{E} = \\ &\quad (\partial_i\partial_j - \frac{1}{3}\delta_{ij}\nabla^2)E - \frac{1}{2}(\partial_i\xi^j + \partial_j\xi^j) + \frac{1}{3}\delta_{ij}\partial_k\xi^k. \end{aligned} \tag{83}$$

When ignoring non-scalar perturbations, gauge transformations introducing vector perturbations are irrelevant. The source of the vector perturbation in such a gauge transformation is the divergenceless part of the Helmholtz decomposition of the

gauge transformation 3-vector ξ^i. Without loss of generality we can therefore ignore the divergenceless part of ξ^i and express the curl-free part in terms of scalar ξ as

$$\xi^i \equiv \delta^{ij}\partial_j \xi \tag{84}$$

when focusing on scalar perturbations. With this, the transformations of the metric perturbations become

$$\tilde{A} = A - \mathcal{H}\xi^0 - \xi^{0\prime}, \tag{85}$$

$$\tilde{B} = B - \xi^0 + \xi', \tag{86}$$

$$\tilde{D} = D + \mathcal{H}\xi^0 + \frac{1}{3}\nabla^2\xi, \tag{87}$$

$$\tilde{E} = E - \xi. \tag{88}$$

There are no constants of integration in (86) and (88) since perturbations average to zero.

With transformations (85) – (88), we are ready to fix the gauge by specifying the gauge transformation parameters ξ^0 and ξ by which one can transition from an arbitrary gauge to the chosen gauge. A desirable goal would be to have a diagonal metric for computational simplicity and that the remaining metric perturbations would be gauge invariant. One suitable set of gauge invariants is the Bardeen potentials [26]:

$$\Phi \equiv A - \mathcal{H}(B + E') - (B + E')' \tag{89}$$

$$\Psi \equiv D + \frac{1}{3}\nabla^2 E + \mathcal{H}(B + E'). \tag{90}$$

If we now perform a gauge transformation with $\xi = E$ and $\xi^0 = E' + B$, from (86) and (88) we see that the metric perturbations B and E vanish in the new gauge. The Bardeen potentials Φ and Ψ are then equal to the remaining metric perturbations A and D, respectively. The perturbed metric is then simply

$$g_{\mu\nu} = a^2(\eta)\begin{pmatrix} -1-2\Phi & 0 \\ 0 & (1-2\Psi)\delta_{ij} \end{pmatrix}. \tag{91}$$

4.3 Perturbations in the Fourier Space

Going to the Fourier space enables us to examine perturbations on different length scales. The convention used in this thesis is to define the Fourier transformation of function $f(t, x^i)$ by

$$f(t, x^i) \equiv \int d^3k\, f(t, k^i) e^{ik_j x^j}. \tag{92}$$

For tensors of different rank, the Fourier transformation is defined similarly.

As has been stated, we are restricting our focus on scalar perturbations. The Fourier transformation of the scalar field v with $v_i^{\mathrm{S}} \equiv \partial_i v$ can be made to have the

same dimension and magnitude as the vector field $v_i^{\rm S}$ by adding an extra $k \equiv \sqrt{k^i k_i}$ in its transformation:

$$v(t, x^i) \equiv \int d^3k \, \frac{v(t, k^i)}{k} e^{ik_j x^j}. \tag{93}$$

For the same reason the Fourier transformation of a scalar field A associated with a symmetric and traceless tensor field A_{ij} through

$$A_{ij}^{\rm S}(t, x^k) = (\partial_i \partial_j - \frac{1}{3}\delta_{ij}\nabla^2) A(t, x^k) \tag{94}$$

carries an additional k^2:

$$A(t, x^i) = \int d^3k \, \frac{A(t, k^i)}{k^2} e^{ik_j x^j}. \tag{95}$$

As x^i are comoving coordinates, k^i is a comoving wave vector. With corresponding physical and comoving wave lengths $\lambda_{\rm phys}$ and λ respectively, the magnitude of the physical wave vector $k^i_{\rm phys}$ relates to k as

$$k_{\rm phys} = \frac{2\pi}{\lambda_{\rm phys}} = \frac{2\pi}{a\lambda} = \frac{k}{a}. \tag{96}$$

The factors of 2π are largely ignored, so that the length scale corresponding to Fourier mode k is just k^{-1}.

A length scale is said to be subhorizontal if a spatial patch of the scale is causally connected. In the converse case the scale is superhorizontal. The Hubble time $H^{-1} = a/\dot{a}$ is a characteristic time scale of the Robertson-Walker metric (24), indicating the time scale on which appreciable expansion occurs. The distance travelled by a light ray in one Hubble time is the Hubble length, also H^{-1} with the speed of light c set to unity. Hence the Hubble length can be taken as the length scale of the causally connected patch. With the comoving Hubble length $(Ha)^{-1} = \mathcal{H}^{-1}$ subhorizontal scales have $k^{-1} < \mathcal{H}^{-1}$, or $k > \mathcal{H}$, while superhorizontal scales are those with $k < \mathcal{H}$.

5 The Perturbation Equations

With the cosmological perturbation theory introduced in section 4, we have the necessary framework for deriving the equations governing the evolution of cosmological perturbations. The derivation starts by establishing the time frame of the structure formation in section 5.1. The composition of the cosmic fluid and the relevant interactions between fluid components during structure formation are also subjects of section 5.1.

In section 5.2, the Einstein equations (6) for the perturbed universe are solved. The Einstein equations relate the metric perturbations Φ and Ψ to the perturbations of the cosmic fluid.

The evolution equations for non-interacting fluid components are derived in section 5.3. The lack of direct interactions with other fluid components makes the derivation quite straightforward, as the energy-momentum continuity can be invoked for the non-interacting components separately.

The section 5.4 contains the most involved derivation of evolution equations presented in this thesis, namely the equations for photons and baryons. Because of the interactions between photons and baryons, the Boltzmann equation is required to describe their evolution. In section 5.4, this is done in detail for photons only. The baryon equations are constructed by utilizing conservation laws and the dark matter equations derived in section 5.3.

Initial values of perturbations are established in section 5.5. Though the initial perturbations are supposedly created by the inflation, the details of the mechanism are not important here. The fact that the initial perturbations are adiabatic is enough for the initial values to be determined once the evolution equations have been derived.

5.1 Fluid Composition during Structure Formation

To specify the composition of the cosmic fluid and the relevant interactions between different components during the time when perturbations evolve, we must determine the time frame of the process.

CMB observations [18] indicate that perturbations on superhorizon scales were adiabatic and nearly scale-invariant in the radiation dominated epoch, presumably as a remnant of the inflation [17]. As is discussed in detail when specifying the initial conditions in section 5.5, the adiabaticity of these primordial perturbations implies that they remain constant on superhorizontal scales or evolve as powers of $k/\mathcal{H} \ll 1$. By and large, the perturbations on scale k therefore start evolving only after the scale crosses the horizon at roughly $k = \mathcal{H}$. From the second Friedmann equation (46) we see that the comoving Hubble length $\mathcal{H}^{-1}$ increases if the cosmic fluid has

$\rho + 3p > 0$, bringing scales into the horizon. Hence the perturbations begin to evolve in the radiation and matter dominated epochs starting from the small scales.

We are interested in length scales upwards from the size of a galaxy, ie. the scale $k_{\mathrm{phys}}^{-1}(t_0) \sim 0.1\,\mathrm{Mpc}$ and larger (see e.g. [28]). The linear perturbation theory is of meager use in explaining the currently observable structures on smaller scales due to growth of perturbations having rendered the perturbative approach invalid so far in the past on those scales (see e.g. [29]). Using the equations (29), (39) and (96) we see that the present day physical scale $k_{\mathrm{phys},0}$ enters the horizon roughly at

$$k_{\mathrm{phys},0} = H_0\sqrt{\Omega_{\mathrm{r}0}(1+z)^2 + \Omega_{\mathrm{m}0}(1+z) + \Omega_{\Lambda 0}(1+z)^{-2}}. \tag{97}$$

Solving z from (97) for $k_{\mathrm{phys},0}^{-1} = 0.1\,\mathrm{Mpc}$ with the cosmological parameter values listed in appendix A results in $z \approx 4.6 \times 10^6$.

From conservation of entropy it follows that after electron-positron annihilations at $T \sim 0.5\,\mathrm{MeV}$ the temperature scales as (see e.g. [30])

$$T \propto \frac{1}{a}. \tag{98}$$

With (29) and (98), temperature corresponding to redshift z is

$$T = (1+z)T_0. \tag{99}$$

Substituting the present day CMB temperature $T_0 = 2.725\,48\,\mathrm{K}$ [31] and $z = 4.6 \times 10^6$ into (99) results in $T \approx 1100\,\mathrm{eV}$. We will therefore consider $T \sim 1\,\mathrm{keV}$ as the starting time point in our structure formation analysis.

The concordance model of cosmology is the ΛCDM model. In the ΛCDM model, there are five components in the cosmic fluid: baryons, cold dark matter, photons, neutrinos and vacuum energy. As is common in the nomenclature of cosmology, baryons are taken to include also electrons (see e.g. [29]). Vacuum energy is homogeneous in the ΛCDM model. (See e.g. [24])

At $T \sim 1\,\mathrm{keV}$, both neutrinos and cold dark matter have decoupled from the plasma (see e.g. [30]), meaning that they interact with other fluid components only through gravitation. We shall approximate neutrinos to be massless. Thus there are two non-interacting components in the fluid: neutrinos that behave as radiation and cold dark matter that behaves as matter.

Electrons with masses $m_{\mathrm{e}} \sim 500\,\mathrm{keV}$ are non-relativistic at $T \sim 1\,\mathrm{keV}$. Because electrons are the lightest particles of what is here called baryons, baryons are non-relativistic during structure formation. Having $T \ll m_{\mathrm{e}}$ also implies that the primary interaction between photons and baryons is Compton scattering of photons and electrons in the low energy limit, or Thomson scattering. Scattering between photons and protons is suppressed in comparison because of the cross section depending on the mass as $\sigma \propto m^{-2}$. A notable feature of the Thomson scattering is that very little energy is transferred between scattering particles. (See e.g. [32])

5.2 The Perturbed Einstein Equations

Using the Einstein equations (6) always proceeds in a similar way: the Einstein tensor $G^{\mu}{}_{\nu}$ is computed from the metric and energy-momentum tensor $T^{\mu}{}_{\nu}$ from fluid properties, and the Einstein equations set a connection between these two tensors. Here the focus will be on the perturbations, as the background Einstein equations result merely in the Friedmann equations (45) and (46). The Einstein equations of interest are therefore

$$\delta G^{\mu}{}_{\nu} = M_{\mathrm{p}}^{-2} \delta T^{\mu}{}_{\nu}. \tag{100}$$

The background Einstein tensor $\bar{G}^{\mu}{}_{\nu}$ is computed with the recipe described in section 2 from the Robertson-Walker metric (43) and the total Einstein tensor from the conformal Newtonian metric (91). The perturbation of the Einstein tensor is simply their difference:

$$\delta G^{\mu}{}_{\nu} = G^{\mu}{}_{\nu} - \bar{G}^{\mu}{}_{\nu}. \tag{101}$$

A straightforward computation reveals that to first order in perturbations

$$\delta G^{0}{}_{0} = 2a^{-2} \left(3\mathcal{H}(\Psi' + \mathcal{H}\Phi) - \nabla^2 \Psi \right) \tag{102}$$

$$\delta G^{i}{}_{0} = 2a^{-2} \partial^{i} \left(\Psi' + \mathcal{H}\Phi \right) \tag{103}$$

$$\delta G^{0}{}_{i} = -\delta G^{i}{}_{0} \tag{104}$$

$$\begin{aligned} \delta G^{i}{}_{j} = {} & a^{-2} \partial^{i} \partial_{j} (\Psi - \Phi) + \\ & a^{-2} \left[2 \left(\Psi'' + \mathcal{H}(\Phi' + 2\Psi') - 3\mathcal{H}^2 w \Phi \right) + \nabla^2 (\Phi - \Psi) \right] \delta^{i}_{j}. \end{aligned} \tag{105}$$

The background energy-momentum tensor $\bar{T}^{\mu}{}_{\nu}$ is necessarily of the perfect fluid form (14) due to isotropy:

$$\bar{T}^{\mu}{}_{\nu} = (\bar{\rho} + \bar{p}) \bar{u}^{\mu} \bar{u}_{\nu} + \bar{p} \delta^{\mu}_{\nu}. \tag{106}$$

The total energy-momentum tensor $T^{\mu}{}_{\nu}$ has the addition of anisotropic stress tensor $\Pi^{\mu}{}_{\nu}$ as per the equation (15):

$$T^{\mu}{}_{\nu} = (\rho + p) u^{\mu} u_{\nu} + p \left(\delta^{\mu}_{\nu} + \Pi^{\mu}{}_{\nu} \right). \tag{107}$$

Keeping only the scalar part of the SVT decomposition of $\Pi^{\mu}{}_{\nu}$, its spatial components can be expressed with a scalar Π as (see e.g. [27])

$$\Pi_{ij} = (\partial_i \partial_j - \frac{1}{3} \delta_{ij} \nabla^2) \Pi. \tag{108}$$

In the background, homogeneity and isotropy set the fluid to be at rest so that the four-velocity of the fluid is $\bar{u}^{\mu} = a^{-1}(1, 0, 0, 0)$. The four-velocity is normalized by $\bar{u}^{\mu} \bar{u}_{\mu} = -1$, so that $\bar{u}_{\mu} = a(-1, 0, 0, 0)$. With a small perturbation the four-velocity can be written as

$$u^{\mu} = \frac{1}{a} \left(1 + a\delta u^0, \partial_1 v, \partial_2 v, \partial_3 v \right) \tag{109}$$

$$u_{\mu} = \left(-a + \delta u_0, \delta u_1, \delta u_2, \delta u_3 \right). \tag{110}$$

Here a velocity perturbation scalar field was defined as $\partial_i v \equiv a u^i$. For the total four-velocity, the normalization implies $\delta u_0 = a^2 \delta u^0$. On the other hand, $u_\mu = g_{\mu\nu} u^\nu$. Combining these with the metric (91) it follows that

$$\delta u^0 = -\frac{\Phi}{a} \tag{111}$$

$$\delta u_i = a\, \partial_i v. \tag{112}$$

With (111) and (112), the four-velocity expressions (109) and (110) become

$$u^\mu = \frac{1}{a}\left(1 - \Phi, \partial_i v\right) \tag{113}$$

$$u_\mu = a\left(-1 - \Phi, \partial_i v\right). \tag{114}$$

With four-velocities resolved, subtracting the background energy-momentum tensor of (106) from the total tensor of (107) gives the perturbation of the energy-momentum tensor:

$$\delta T^0{}_0 = -\delta\rho \tag{115}$$

$$\delta T^i{}_0 = -(\bar{\rho} + \bar{p})\partial^i v \tag{116}$$

$$\delta T^0{}_i = -\delta T^i{}_0 \tag{117}$$

$$\delta T^i{}_j = \delta p \delta^i_j + \bar{p}\left(\partial^i \partial_j - \frac{1}{3}\delta^i_j \nabla^2\right)\Pi. \tag{118}$$

The Einstein equations (100) can now be used to relate perturbation of the Einstein tensor $\delta G^\mu{}_\nu$ with the perturbation of the energy-momentum tensor $\delta T^\mu{}_\nu$. For $\delta G^0{}_0$ from (102) and $\delta T^0{}_0$ from (115) the Einstein equations yield

$$3\mathcal{H}(\Psi' + \mathcal{H}\Phi) - \nabla^2\Psi = -\frac{3}{2}\mathcal{H}^2\delta. \tag{119}$$

In the equation (119), δ is the density contrast, defined as

$$\delta \equiv \frac{\delta\rho}{\bar{\rho}} = \frac{\rho}{\bar{\rho}} - 1. \tag{120}$$

The Friedmann equation (45) was also used to simplify the equation (119).

Taking $\delta G^i{}_0$ from (103) and $\delta T^i{}_0$ from (116) and applying the Einstein equations gives

$$\partial_i(\Psi' + \mathcal{H}\Phi) = -\frac{3}{2}(1+w)\mathcal{H}^2\, \partial_i v. \tag{121}$$

In (121), the equation of state parameter w is defined with respect to background quantities,

$$w \equiv \frac{\bar{p}}{\bar{\rho}}. \tag{122}$$

Because perturbations average to zero, equal gradients of perturbative quantities mean that the quantities themselves must be equal. From (121) then follows

$$\Psi' + \mathcal{H}\Phi = -\frac{3}{2}(1+w)\mathcal{H}^2\, v. \tag{123}$$

For relations resulting from $\delta G^i{}_j$ and $\delta T^i{}_j$ components, it is convenient to separate the respective matrices to their traces and trace-free parts. For the traces, the Einstein equations set $\delta G^i{}_i = M_{\rm p}^{-2}\,\delta T^i{}_i$, so that with (105) and (118)

$$\Psi'' + \mathcal{H}(\Phi' + 2\Psi') - 3w\mathcal{H}^2\Phi + \frac{1}{3}\nabla^2(\Phi - \Psi) = \frac{3}{2}\mathcal{H}^2\frac{\delta p}{\bar{\rho}}. \tag{124}$$

The Einstein equations applied to the trace-free parts give

$$\delta G^i{}_j - \frac{1}{3}\delta G^k{}_k\delta^i_j = M_{\rm p}^{-2}(\delta T^i{}_j - \frac{1}{3}\delta T^k{}_k\delta^i_j), \tag{125}$$

or with (105) and (118):

$$(\partial_i\partial_j - \frac{1}{3}\delta_{ij}\nabla^2)(\Psi - \Phi) = 3w\mathcal{H}^2(\partial_i\partial_j - \frac{1}{3}\delta_{ij}\nabla^2)\Pi. \tag{126}$$

Again invoking the fact that perturbations average to zero it follows from (126) that

$$\Psi - \Phi = 3w\mathcal{H}^2\Pi. \tag{127}$$

The final set of Einstein equations is then equations (119), (123), (124) and (127). In Fourier space, these read

$$3\mathcal{H}^{-1}(\Psi' + \mathcal{H}\Phi) + \left(\frac{k}{\mathcal{H}}\right)^2\Psi = -\frac{3}{2}\delta \tag{128}$$

$$\mathcal{H}^{-1}\Psi' + \Phi = -\frac{3}{2}(1+w)\frac{\mathcal{H}}{k}v \tag{129}$$

$$\mathcal{H}^{-2}\Psi'' + \mathcal{H}^{-1}(\Phi' + 2\Psi') - 3w\Phi + \frac{1}{3}\left(\frac{k}{\mathcal{H}}\right)^2(\Psi - \Phi) = \frac{3}{2}\frac{\delta p}{\bar{\rho}} \tag{130}$$

$$\Psi - \Phi = 3w\left(\frac{\mathcal{H}}{k}\right)^2\Pi. \tag{131}$$

5.3 Non-Interacting Fluid Components

As stated in section 5.1, neutrinos and dark matter have decoupled from the cosmic plasma by the time when scales relevant to large scale structure formation start to enter the horizon. As a result, neutrinos and dark matter both evolve freely with no transfer of energy or momentum with other fluid components. Therefore these components satisfy separate energy-momentum continuities (19):

$$\nabla_\mu(T_i)^\mu{}_\nu = 0, \tag{132}$$

with i being either c for cold dark matter or ν for neutrinos.

In the unperturbed background, $\nabla_\mu(T_i)^\mu{}_0 = 0$ results in the FRW continuity equation (32). Using this result, $\nabla_\mu(T_i)^\mu{}_0 = 0$ up to first order in perturbations results in

$$(\delta\rho_i)' = -3\mathcal{H}(\delta\rho_i + \delta p_i) + (\bar{\rho}_i + \bar{p}_i)(3\Psi' - \nabla^2 v_i). \tag{133}$$

With the density contrast (120) this can be recast as

$$\delta_i' = 3\mathcal{H}\left(w_i\delta_i - \frac{\delta p_i}{\bar{\rho}_i}\right) + (1+w_i)(3\Psi' - \nabla^2 v_i). \tag{134}$$

The rest of the continuity equations, $\nabla_\mu (T_i)^\mu{}_j = 0$, result in

$$\partial_j\left((\bar{\rho}_i' + \bar{p}_i')v_i + (\bar{\rho}_i + \bar{p}_i)\left(v_i' + 4\mathcal{H}v_i + \Phi\right) + \delta p_i + \frac{2}{3}\bar{p}_i\nabla^2\Pi_i\right) = 0. \tag{135}$$

Since everything inside the parenthesis is perturbative and perturbations average to zero, the term inside the parenthesis must be zero. Solving v_i' gives

$$v_i' = \left(\mathcal{H}(3w_i - 1) - \frac{w_i'}{1+w_i}\right)v_i - \frac{\delta p_i}{\bar{\rho}_i + \bar{p}_i} - \frac{2}{3}\frac{w_i}{1+w_i}\nabla^2\Pi_i - \Phi. \tag{136}$$

Approximating neutrinos to be massless, their equation of state is $p_\nu = \rho_\nu/3$. Equations (134) and (136) then give

$$\delta_\nu' = -\frac{4}{3}\nabla^2 v_\nu + 4\Psi' \tag{137}$$

$$v_\nu' = -\frac{1}{4}\delta_\nu - \frac{1}{6}\nabla^2\Pi_\nu - \Phi. \tag{138}$$

Cold dark matter has no pressure, so

$$\delta_\mathrm{c}' = -\nabla^2 v_\mathrm{c} + 3\Psi' \tag{139}$$

$$v_\mathrm{c}' = -\mathcal{H}v_\mathrm{c} - \Phi. \tag{140}$$

In Fourier space these read

$$\delta_\nu' = \frac{4}{3}kv_\nu + 4\Psi' \tag{141}$$

$$v_\nu' = -\frac{1}{4}k\delta_\nu + \frac{1}{6}k\Pi_\nu - k\Phi \tag{142}$$

$$\delta_\mathrm{c}' = kv_\mathrm{c} + 3\Psi' \tag{143}$$

$$v_\mathrm{c}' = -\mathcal{H}v_\mathrm{c} - k\Phi. \tag{144}$$

The evolution equations for photons and baryons, derived in the next section, are similar to those of neutrinos and dark matter respectively, only with interaction terms added. An equation for the neutrino anisotropic stress Π_ν is also needed to gain a complete set of differential equations. That equation will be derived as a side result of photon equations.

5.4 Photons and Baryons

As was established in section 5.1, the primary interaction between baryons and photons during structure formation is the Thomson scattering between low-energy photons ($T \ll m_\mathrm{e}$) and non-relativistic electrons:

$$e^-(\mathbf{p}_\mathrm{e}) + \gamma(\mathbf{p}_\gamma) \leftrightarrow e^-(\mathbf{p}'_\mathrm{e}) + \gamma(\mathbf{p}'_\gamma). \tag{145}$$

In Thomson scattering, there is essentially no transfer of energy between electrons and photons, so that only the three-momentum p^i of the particles is changed (see e.g. [32]). Electrons and protons are held in equilibrium by their electromagnetic interactions and hence protons are also affected by the scattering process.

Because of scatterings, the evolution equations for photons and baryons must be derived starting from the Boltzmann equation (see e.g. [33])

$$\frac{df}{d\eta} = C[f]. \tag{146}$$

The Boltzmann equation states that scattering, manifesting in the collision term C, changes the phase space distribution f of the particle species. The collision term is computed with basic particle physics machinery using Feynman rules. In the following derivation of the Boltzmann equation for photons, the collision term will be taken from literature. The baryon equations can be derived using the photon equations and conservation of momentum in the scattering.

As will be seen in section 5.4.4, the Boltzmann equation for photons results in an infinite series of differential equations for multipoles of the photon brightness function. This presents a problem for a numerical solution of the perturbation equations as some approximation must be made to truncate the series. A truncation scheme with some degree of justification is presented in section 5.4.4.

5.4.1 The Distribution Function

The phase space distribution $f(\eta, x^i, p^i)$ measures the number of particles within the phase space volume $d^3x\, d^3p$ at time η so that if N is the number of particles

$$dN \equiv \frac{g}{(2\pi)^3} f(\eta, x^i, p^i) d^3x\, d^3p. \tag{147}$$

The prefactor $g/(2\pi)^3$ with the number of internal degrees of freedom g is the density of states. For photons with two spin states $g = 2$.

The distribution f is a Lorentz scalar (see e.g. [34]), so that we are free to choose the coordinate system. It will be convenient to take the momentum to be that measured by a comoving observer. Let q be the measured photon energy. The frame in which q is the zero component of the photon four-momentum $p^{\hat{\mu}} = dx^{\hat{\mu}}/d\lambda$ is the local orthonormal frame at the point of observation (see e.g. [35]). This is because in the local orthonormal frame the photon energy can be expressed using the observer four-velocity $u^{\hat{\mu}} = (1, 0, 0, 0)$ as

$$q = -\eta_{\hat{\mu}\hat{\nu}} p^{\hat{\mu}} u^{\hat{\nu}} = p^{\hat{0}}. \tag{148}$$

The observed three-momentum is then $q^i = qn^i = p^{\hat{i}}$, with n^i being a unit vector in direction of the momentum. The suitable variables for the distribution function are now set with $f = f(\eta, x^i, q, n^i)$.

In the end, we would like to discuss the perturbations in the photon fluid in terms of density contrast δ and velocity perturbation v as was done with the fluid as a whole and its non-interacting components in sections 5.2 and 5.3 respectively. Relating the distribution function to the fluid quantities can be done through the energy-momentum tensor.

In the local orthonormal frame, the energy-momentum tensor can be expressed as (see e.g. [34])

$$T^{\hat{\mu}}{}_{\hat{\nu}} = \frac{g}{(2\pi)^3} \int \frac{d^3p}{p^{\hat{0}}} f p^{\hat{\mu}} p_{\hat{\nu}}. \tag{149}$$

In the coordinate frame, the energy-momentum tensor of photons is of the same form as for the whole fluid:

$$T^0{}_0 = -\rho \tag{150}$$
$$T^0{}_i = (\bar{\rho} + \bar{p})\partial_i v \tag{151}$$
$$T^i{}_0 = -\delta T^0{}_i \tag{152}$$
$$T^i{}_j = p\delta^i_j + \bar{p}\Pi^i{}_j \tag{153}$$

as seen in equations (106) and (115) – (118). By inspection of the metric (91) the transformation between the coordinate frame and the local orthonormal frame is

$$\frac{\partial x^\mu}{\partial x^{\hat{\nu}}} = \frac{1}{a} \begin{pmatrix} 1 - \Phi & \\ & (1 + \Psi)\delta_{ij} \end{pmatrix}. \tag{154}$$

Transforming the photon energy-momentum tensor to the local orthonormal frame results in

$$T^{\hat{\mu}}{}_{\hat{\nu}} = \frac{\partial x^{\hat{\mu}}}{\partial x^\alpha} \frac{\partial x^\beta}{\partial x^{\hat{\nu}}} T^\alpha{}_\beta = T^\mu{}_\nu. \tag{155}$$

A relation this simple holds only up to first order in perturbations.

The connections between the distribution and the fluid quantities are then (with $p^{\hat{\mu}} = q^\mu$)

$$\rho = \frac{g}{(2\pi)^3} \int d^3q\, fq \tag{156}$$
$$(\bar{\rho} + \bar{p})\partial_i v = \frac{g}{(2\pi)^3} \int d^3q\, fqn^i \tag{157}$$
$$\bar{p}\Pi^i{}_j = \frac{g}{(2\pi)^3} \int d^3q \left(n^i n_j - \frac{1}{3}\delta^i_j \right) fq. \tag{158}$$

5.4.2 Expanding the $df/d\eta$ Term

The derivative of the distribution function $f = f(\eta, x^i, q, n^i)$ with respect to conformal time η can be expanded with the chain rule:

$$\frac{df}{d\eta} = \frac{\partial f}{\partial \eta} + \frac{\partial f}{\partial x^i}\frac{dx^i}{d\eta} + \frac{\partial f}{\partial q}\frac{dq}{d\eta} + \frac{\partial f}{\partial n^i}\frac{dn^i}{d\eta}. \tag{159}$$

In the homogeneous and isotropic background universe, the distribution has no dependence on location x^i or direction n^i, making $\partial f/\partial x^i$ and $\partial f/\partial n^i$ first order quantities. A collisionless change in the direction of the photon requires a non-homogeneous energy density, making $dn^i/d\eta$ a first order term. The last term in (159) is therefore second order and is neglected.

With the chain rule, $dx^i/d\eta$ can be expressed in terms of photon four-momentum $p^\mu = dx^\mu/d\lambda$:

$$\begin{aligned}\frac{dx^i}{d\eta} &= \frac{dx^i}{d\lambda}\frac{d\lambda}{d\eta} \\ &= \frac{p^i}{p^0}.\end{aligned} \tag{160}$$

Transforming the photon four-momentum from the local orthonormal frame to the coordinate frame with (154) gives

$$p^\mu = \frac{q}{a}(1 - \Phi, (1 + \Psi)n^i). \tag{161}$$

Because in (159) $dx^i/d\eta$ is multiplied by the first-order term $\partial f/\partial x^i$, only zeroth order terms of $dx^i/d\eta$ are relevant. From (160) and (161) we get to zeroth order

$$\frac{dx^i}{d\eta} \approx n^i. \tag{162}$$

The photon energy as measured by the comoving observer is $q = -p^{\hat{\mu}}u_{\hat{\mu}} = -p^\mu u_\mu$ as stated in (148). Its derivative with respect to conformal time is then

$$\frac{dq}{d\eta} = -p^\mu\frac{du_\mu}{d\eta} - u_\mu\frac{dp^\mu}{d\eta}. \tag{163}$$

Up to first order in perturbations

$$\frac{du_\mu}{d\eta} = \frac{\partial u_\mu}{\partial \eta} + \frac{\partial u_\mu}{\partial x^i}n^i. \tag{164}$$

In (164), the zeroth order expression (162) was used since $\partial u_\mu/\partial x^i$ is a first order term. With the metric (91) the four-velocity of a comoving observer is

$$\begin{aligned}u^0 &= \frac{1}{a}(1 - \Phi) \\ u^i &= 0.\end{aligned} \tag{165}$$

The corresponding dual vector is then

$$\begin{aligned} u_0 &= -a(1+\Phi) \\ u_i &= 0. \end{aligned} \tag{166}$$

With (161), (164) and (166), the first term on the right hand side of the equation (163) is

$$p^\mu \frac{du_\mu}{d\eta} = -q\left(\mathcal{H} + \Phi' + n^i \partial_i \Phi\right). \tag{167}$$

In (163), $dp^\mu/d\eta$ is contracted with u_μ. Since $u_i = 0$, only the zero component of $dp^\mu/d\eta$ is relevant. With the chain rule

$$\frac{dp^0}{d\eta} = \frac{1}{p^0}\frac{dp^0}{d\lambda}. \tag{168}$$

From the geodesic equation (23) we get

$$\frac{dp^0}{d\lambda} = -\Gamma^0_{\rho\sigma} p^\rho p^\sigma. \tag{169}$$

Computing the connections $\Gamma^0_{\rho\sigma}$ from the metric (91) and taking the observer four-velocity and the photon four-momentum from (166) and (161) respectively results in

$$u_\mu \frac{dp^\mu}{d\eta} = u_0 \frac{dp^0}{d\eta} = q\left(2\mathcal{H} + \Phi' - \Psi' + 2n^i \partial_i \Phi\right). \tag{170}$$

With (167) and (170), the equation (163) becomes

$$\frac{dq}{d\eta} = -q(\mathcal{H} - \Psi' + n^i\, \partial_i \Phi). \tag{171}$$

At this point, the left hand side of the Boltzmann equation (146) for photons can be expressed as

$$\frac{df}{d\eta} = \frac{\partial f}{\partial \eta} + n^i \partial_i f - q\frac{\partial f}{\partial q}(\mathcal{H} - \Psi' + n^i\, \partial_i \Phi). \tag{172}$$

The perturbations enter as the last two terms inside the parenthesis in (172). These terms encode the effects of gravitational red- and blueshift on photons, whereas the term proportional to $\mathcal{H}$ describes redshift due to expansion of the universe.

In a homogeneous and isotropic universe, the second term on the right hand side of (172) vanishes, as well as the two last terms inside the parenthesis. In the background universe, the photons distribution maintains their equilibrium form and the collision term of the Boltzmann equation (146) is zero:

$$\frac{d\bar{f}}{d\eta} = \frac{\partial \bar{f}}{\partial \eta} - q\frac{\partial \bar{f}}{\partial q}\mathcal{H} = 0. \tag{173}$$

Equation (173) results in the continuity equation (32) with the equation (156), which relates the energy density to the distribution function. Using the equations (172) and (173) and dividing the distribution into background and perturbation $f = \bar{f} + \delta f$ makes $df/d\eta$ depend solely on perturbations:

$$\frac{df}{d\eta} = \frac{d(\delta f)}{d\eta} = \frac{\partial(\delta f)}{\partial\eta} + n^i\partial_i(\delta f) - q\frac{\partial(\delta f)}{\partial q}\mathcal{H} + q\frac{\partial\bar{f}}{\partial q}(\Psi' - n^i\partial_i\Phi). \tag{174}$$

Thus far nothing has been stated about the distribution function f that is specific to photons. Giving an expression to the distribution function is the subject of the next section.

5.4.3 The Brightness Function

In the background universe the photon distribution is independent of location and direction. Since photons are bosons, their background distribution is of the Bose-Einstein form:

$$\bar{f}(\eta, q) = \frac{1}{e^{q/T(\eta)} - 1}. \tag{175}$$

The only type of deviation from the background distribution form (175) that has been observed in the cosmic microwave background is the fluctuation of temperature [36, 37]. The temperature contrast $\delta T/T$ is commonly known as the brightness function Θ (see e.g. [35]):

$$\Theta \equiv \frac{\delta T}{T}. \tag{176}$$

In this notation T always refers to the background temperature. What it means for the brightness function Θ to be a perturbation of the temperature is that it does not change the functional form of the energy distribution as described by the Bose-Einstein distribution (175). Therefore Θ does not depend of the photon energy. With the addition of Θ, the distribution of photons is

$$f(\eta, x^i, q, n^i) = \frac{1}{\exp\left(\frac{q}{T(\eta)(1+\Theta(\eta,x^i,n^i))}\right) - 1}. \tag{177}$$

The types of perturbations omitted from the distribution (177) are known as spectral distortions. Spectral distortions come in two flavors: those introducing a non-zero photon chemical potential μ and those that make the distribution deviate from the Bose-Einstein form. Setting $\mu = 0$ implies assuming that photon number changing processes, most notably double Compton scattering and bremsstrahlung, are effective in keeping the number of photons at a given temperature at the blackbody value. Sustaining the Bose-Einstein form on the other hand is the result of the Thomson scattering being able to keep the photons in kinetic equilibrium. The spectrum of CMB is predicted to be slightly distorted, but to such a small degree that the distortions are beyond the current precision of observations [38]. [39–41]

The distribution f of (177) can be divided into background and perturbation as $f = \bar{f} + \delta f$ with the perturbation δf depending on the brightness function Θ. Expanding the distribution around the background temperature T gives

$$f = \bar{f} + \frac{\partial \bar{f}}{\partial T}\delta T. \tag{178}$$

Since $\Theta = \delta T/T$, the perturbation of the distribution can be identified as

$$\delta f = \frac{\partial \bar{f}}{\partial T} T\Theta. \tag{179}$$

The background distribution function $\bar{f}$ of (175) is a function of q/T, so

$$T\frac{\partial \bar{f}}{\partial T} = -q\frac{\partial \bar{f}}{\partial q}. \tag{180}$$

With (179) and (180), the perturbation can be expressed without explicitly referring to the temperature as

$$\delta f = -q\frac{\partial \bar{f}}{\partial q}\Theta. \tag{181}$$

In Fourier space, the brightness function can be conveniently connected to the density contrast δ and velocity perturbation v of the fluid. To this end, the l:th multipole of the brightness function is defined by expansion with Legendre polynomials P_l (see e.g. [42]):

$$\Theta(\eta, k^i, n^i) = \sum_l (-i)^l (2l+1) P_l(\cos\theta)\Theta_l(\eta, k^i). \tag{182}$$

In the expansion the photon direction n^i is expressed through its angle with the Fourier mode k^i:

$$\cos\theta \equiv \frac{k_i n^i}{k}. \tag{183}$$

Using the orthogonality relation of the Legendre polynomials

$$\int_{-1}^{1} dx P_l(x) P_k(x) = \frac{2}{2l+1}\delta_{lk} \tag{184}$$

the multipole Θ_l can be solved from (182):

$$\Theta_l(\eta, k^i) = \frac{i^l}{2}\int_{-1}^{1} d\cos\theta\, P_l(\cos\theta)\Theta(\eta, k^i, n^i). \tag{185}$$

Switching to solid angle integral, (185) becomes

$$\Theta_l(\eta, k^i) = \frac{i^l}{4\pi}\int d\Omega\, P_l(\cos\theta)\Theta(\eta, k^i, n^i). \tag{186}$$

Taking the expression for energy density in terms of the distribution from (156), relating the perturbation of the distribution to the brightness function with (181) and using (186) results in

$$\delta = \frac{\delta\rho}{\bar{\rho}} = 4\Theta_0. \tag{187}$$

Similarly with the used Fourier convention for the velocity perturbation v and anisotropic stress Π the equations (157) and (158) yield

$$v = -3\Theta_1 \tag{188}$$

$$\Pi = 12\Theta_2. \tag{189}$$

5.4.4 The Boltzmann Hierarchy

The equation (174) gives an expression for $df/d\eta$ in terms of the perturbation of the distribution δf, and (181) relates δf to the brightness function. Combining these yields

$$\frac{df}{d\eta} = -q\frac{\partial \bar{f}}{\partial q}\left(\Theta' + n^i\partial_i\Theta - \Psi' + n^i\partial_i\Phi\right). \tag{190}$$

In Fourier space

$$\frac{df}{d\eta} = -q\frac{\partial \bar{f}}{\partial q}\left(\Theta' + ik\Theta\cos\theta - \Psi' + ik\Phi\cos\theta\right). \tag{191}$$

The collision term $C[f]$ in the Boltzmann equation (146) describes the effect of Thomson scattering (145) on the distribution function. In equilibrium, the forward and backward reactions of (145) balance each other and the collision term is zero. In non-equilibrium state the collision term must be computed using the standard particle physics toolkit. The calculation can be found for example in [29]. The resulting approximate collision term is in Fourier space

$$C[f] = -q\frac{\partial \bar{f}}{\partial q}an_{\mathrm{e}}\sigma_{\mathrm{T}}\left(\Theta_0 - \Theta + v_{\mathrm{b}}\cos\theta - \frac{1}{2}P_2(\cos\theta)\Theta_2\right). \tag{192}$$

In (192) n_{e} is the free electron number density, σ_{T} the Thomson cross-section and v_{b} the baryon velocity perturbation. The evolution of n_{e} is discussed in section 5.4.6.

The collision term of (192) is an approximation which ignores the effect of polarization, which affects the invariant amplitude of the scattering (see e.g. [29]). The polarization effects are small corrections to the collision term but of significant physical interest since they introduce a method alternative to temperature anisotropy measurements in probing the CMB. For a treatment including the polarization effects, see e.g. [43].

The Boltzmann equation (146) equates $df/d\eta$ from (191) and the collision term (192). The prefactors cancel, leaving

$$\begin{aligned}\Theta' + ik\Theta\cos\theta - \Psi' + ik\Phi\cos\theta = \\ an_{\mathrm{e}}\sigma_{\mathrm{T}}\left(\Theta_0 - \Theta + iv_{\mathrm{b}}\cos\theta - \frac{1}{2}P_2(\cos\theta)\Theta_2\right).\end{aligned} \tag{193}$$

The equation (193) can be turned into an equation of multipoles Θ_l by integrating both sides with $\frac{i^l}{2}\int_{-1}^{1} d\cos\theta\, P_l(\cos\theta)$ and using the orthogonality relation (184) as well as the recursive formula

$$(l+1)P_{l+1}(x) = (2l+1)xP_l(x) - lP_{l-1}(x) \tag{194}$$

of Legendre polynomials. The resulting equation is

$$\begin{aligned}\Theta_l' + \frac{k}{2l+1}((l+1)\Theta_{l+1} - l\Theta_{l-1}) - \frac{1}{3}k\Phi\delta_{l1} - \Psi'\delta_{l0} = \\ n_{\mathrm{e}}\sigma_T a\left(\Theta_0\delta_{l0} - \Theta_l - \frac{1}{3}v_{\mathrm{b}}\delta_{l1} + \frac{1}{10}\Theta_2\delta_{l2}\right).\end{aligned} \tag{195}$$

Equation (195) is called the Boltzmann hierarchy of photons. In terms of fluid quantities it can be recast with (187) – (189) as

$$\delta_\gamma' = \frac{4}{3}kv_\gamma + 4\Psi' \tag{196}$$

$$v_\gamma' = -\frac{1}{4}k\delta_\gamma + \frac{1}{6}k\Pi_\gamma - k\Phi + n_{\mathrm{e}}\sigma_{\mathrm{T}}a(v_{\mathrm{b}} - v_\gamma) \tag{197}$$

$$\Pi_\gamma' = -\frac{36}{5}k\Theta_3 - \frac{8}{5}kv_\gamma - \frac{9}{10}n_{\mathrm{e}}\sigma_{\mathrm{T}}a\Pi_\gamma \tag{198}$$

$$\Theta_l' = \frac{k}{2l+1}(l\Theta_{l-1} - (l+1)\Theta_{l+1}) - n_{\mathrm{e}}\sigma_T a\Theta_l, \qquad l \geq 3. \tag{199}$$

Specifying the fluid component in the subscript has been reinstated in (196) – (198) to make the fluid equations of photons consistent with those of neutrinos and dark matter seen in section 5.3.

The Boltzmann hierarchy establishes the coupling between different multipoles up to infinite l. Numerical solutions of the photon perturbations therefore require truncating the hierarchy at some multipole $l_{\max}$. A first approximation, used for example in [44] and [45], would be to set all higher multipoles to zero :

$$\Theta_l = 0, \qquad l > l_{\max}. \tag{200}$$

From (189) it can be seen that approximating the photons to behave as a perfect fluid is equivalent with using the truncation scheme of (200) with $l_{\max} = 1$.

Using (199) with the truncation scheme (200), the derivative of the multipole $l_{\max+1}$ is

$$\Theta_{l_{\max}+1}' = \frac{k}{2l_{\max}+3}(l_{\max}+1)\Theta_{l_{\max}} \tag{201}$$

for $l_{\max} \geq 2$. Forcing $\Theta_{l_{\max}+1} = 0$ as per (200) therefore contradicts the Boltzmann hierarchy if $\Theta_{l_{\max}} \neq 0$. By ignoring the transfer of power from multipoles $l \leq l_{\max}$ to multipoles $l > l_{\max}$, the simple truncation scheme (200) exaggerates the examined perturbations [46].

In [42] a less arbitrary truncation scheme is offered. With the added assumption of $\Phi' + \Psi' = 0$ the multipole Θ_l can be shown to be proportional to spherical Bessel function $j_l(k\eta)$. With the recursion relation of spherical Bessel functions

$$(2l+1)j_l = x\left(j_{l+1}(x) + j_{l-1}(x)\right) \tag{202}$$

the $l_{\max}+1$ multipole can be approximated to be [42]

$$\Theta_{l_{\max}+1} \approx \frac{2l_{\max}+1}{k\eta}\Theta_{l_{\max}} - \Theta_{l_{\max}-1}. \tag{203}$$

In the Boltzmann hierarchy (195), the evolution equation of multipole Θ_l involves only multipoles $l-1$, l and $l+1$. Specifying $\Theta_{l_{\max}+1}$ in terms of $\Theta_{l_{\max}-1}$ and $\Theta_{l_{\max}}$ by (203) is therefore sufficient to truncate the Boltzmann hierarchy to a closed set of coupled differential equations.

Though improving the correspondence between numerical solutions and observations compared to the naive truncation of (200), the truncation scheme of (203) is a fairly crude approximation especially for low $l_{\max}$ [42]. Especially in the radiation dominated epoch the perturbations of the metric Φ and Ψ vary rapidly, as can be seen from numerical solutions in section 6.2.

For massless neutrinos, the Boltzmann equation results in hierarchy similar to (196) – (199), only without the interaction terms. Indeed, the neutrino equations (141) and (142) derived from energy-momentum continuity are identical to equations (196) and (197) with the interaction term removed. The equation for the neutrino anisotropic stress Π_ν is therefore

$$\Pi_\nu' = -\frac{36}{5}k(\Theta_\nu)_3 - \frac{8}{5}kv_\nu \tag{204}$$

with the higher multipoles evolving as

$$(\Theta_\nu)_l' = \frac{k}{2l+1}(l(\Theta_\nu)_{l-1} - (l+1)(\Theta_\nu)_{l+1}), \qquad l \geq 3. \tag{205}$$

5.4.5 The Baryon Equations

For the purpose of this discussion, the only difference between baryonic and dark matter is that baryons interact with photons through Thomson scattering (145), whereas dark matter is decoupled from the plasma in the examined time period. The baryon equations can therefore be constructed by adding an interaction term to the dark matter equations (143) and (144).

Transfer of energy is insignificant in the low-energy Thomson scattering (see e.g. [32]). Therefore the density contrast has no direct dependence on interactions, making its evolution equation for baryons identical to that of dark matter

$$\delta_{\mathrm{b}}' = kv_{\mathrm{b}} + 3\Psi'. \tag{206}$$

Momentum is conserved in the scattering. For collisional contributions to v' this means that

$$(\bar{\rho}_{\mathrm{b}} + \bar{p}_{\mathrm{b}})v_{\mathrm{b,coll}}' = -(\bar{\rho}_\gamma + \bar{p}_\gamma)v_{\gamma,\mathrm{coll}}'. \tag{207}$$

Taking v_γ' from (197) and using the equations of state $\bar{p}_{\mathrm{b}} = 0$ and $\bar{p}_\gamma = \bar{\rho}_\gamma/3$, we get the collision term for baryon velocity perturbation

$$v_{\mathrm{b,coll}}' = \frac{4}{3}\frac{\bar{\rho}_\gamma}{\bar{\rho}_{\mathrm{b}}} n_{\mathrm{e}}\sigma_{\mathrm{T}} a(v_\gamma - v_{\mathrm{b}}). \tag{208}$$

The non-collisional part of v_b' is identical to v_c', so that with (144)

$$v_\mathrm{b}' = -\mathcal{H}v_\mathrm{b} - k\Phi + \frac{4}{3}\frac{\bar{\rho}_\gamma}{\bar{\rho}_\mathrm{b}} n_\mathrm{e}\sigma_\mathrm{T} a(v_\gamma - v_\mathrm{b}). \tag{209}$$

5.4.6 Recombination

To get a complete set of equations describing the evolution of perturbations we still need an equation for the free electron number density n_e. Free electron number density makes an appearance in the interaction terms of equations (197) – (199) and (209).

The density of free electrons depends on the amount of electrons bound in atoms. At temperatures $T \gtrsim 1\,\mathrm{eV}$, all electrons are free due to large number of high energy photons instantly ionizing all forming atoms. As temperature drops, a growing amount of electrons is able to combine with nuclei. This process is known as the recombination. (See e.g. [29])

For this discussion, the only recombination process considered will be the formation and ionization of hydrogen

$$p^+ + e^- \leftrightarrow H + \gamma. \tag{210}$$

We are thus ignoring the subdominant recombination processes, most notably that of helium [46, 47]. Deriving the evolution of n_e is further simplified by noting that in the fluid equations n_e appears in ((197) – (199) and (209)) it is multiplied by first order perturbations. It is therefore sufficient to examine n_e in the homogeneous background universe.

We shall start by defining the free electron fraction X_e as the ratio of free electron number density n_e and the number density of all electrons n_e^*:

$$X_\mathrm{e} \equiv \frac{n_\mathrm{e}}{n_\mathrm{e}^*}. \tag{211}$$

Because the universe is electrically neutral, the total number density of electrons matches that of protons, $n_\mathrm{e}^* = n_\mathrm{p}^*$. In the time frame of structure formation the temperature is below $T \sim 1\,\mathrm{keV}$ at which point baryons[1] are predominantly protons due to them being the lightest baryon species (see e.g. [29]). Hence we approximate $n_\mathrm{b} \approx n_\mathrm{p}^*$. The free electron number density is thus

$$n_\mathrm{e} = X_\mathrm{e} n_\mathrm{b}. \tag{212}$$

First we shall see how the free electron fraction X_e evolves in thermodynamic equilibrium. In equilibrium, the distribution function f of photons is of the Bose-Einstein form (175). By definition (147), the distribution function relates to number density n as

$$n = \frac{g}{(2\pi)^3}\int f\, d^3p. \tag{213}$$

[1]When discussing recombination, "baryons" are defined in the normal particle physics manner, i.e. electrons are not included.

Substituting f from (175) into (213) and integrating yields the number density of photons in thermodynamic equilibrium:

$$n_\gamma = \frac{2\zeta(3)}{\pi^2} T^3, \tag{214}$$

where ζ is the Riemann zeta function.

The conservation of baryon number implies that their number density scales as $n_\mathrm{b} \propto a^{-3}$. With $a \propto T^{-1}$ as established in (98), we get the temperature dependence of n_b:

$$n_\mathrm{b} \propto T^3, \tag{215}$$

valid from the electron-positron annihilations to the present day. From (214) and (215) we see that in the discussed time frame the ratio of baryon and photon number densities is a constant. Defining η_B to be the present day ratio

$$\eta_\mathrm{B} \equiv \frac{n_\mathrm{b}(t_0)}{n_\gamma(t_0)} \tag{216}$$

and using (214) yields

$$n_\mathrm{b} = \eta_\mathrm{B} \frac{2\zeta(3)}{\pi^2} T^3. \tag{217}$$

Observations indicate that $\eta_\mathrm{B} \approx 6.07 \times 10^{-10}$ [48].

Another relation n_b fulfills can be found by considering the distribution function of non-relativistic particles. In general, the distribution is

$$f = \frac{1}{e^{(E-\mu)/T} \pm 1} \tag{218}$$

with plus sign for fermions and minus for bosons. In (218), $E = \sqrt{m^2 + p^2}$ is the energy and μ is the chemical potential. Since $p \ll m$ for non-relativistic particles, the energy can be approximated as

$$E \approx m + \frac{p^2}{2m}. \tag{219}$$

For a sufficiently dilute system of massive particles $m - \mu \gg T$ (see e.g. [49]). Then the denominator in (218) is dominated by the exponential term and so

$$f \approx \exp(-\frac{p^2}{2mT} - \frac{m-\mu}{T}). \tag{220}$$

The distribution of non-relativistic particles then makes no distinction between fermions and bosons. The number density is given by (213) and (220):

$$n = g \left(\frac{mT}{2\pi}\right)^{3/2} e^{-(m-\mu)/T}. \tag{221}$$

The equation (221) expresses the number density of a massive particle species as a function of their temperature T and chemical potential μ. While the recombination

reaction (210) is in chemical equilibrium, the chemical potentials of the involved particles have the relation

$$\mu_{\rm p} + \mu_{\rm e} = \mu_{\rm H} + \mu_\gamma, \tag{222}$$

where the chemical potential of photons $\mu_\gamma = 0$ (see e.g. [49]). Combining (221) and (222) implies

$$\frac{n_{\rm H}}{n_{\rm p} n_{\rm e}} = \left(\frac{2\pi}{m_{\rm e} T}\right)^{3/2} e^{B_{\rm H}/T}. \tag{223}$$

Here $B_{\rm H} = m_{\rm p} + m_{\rm e} - m_{\rm H} = 13.6\,{\rm eV}$ is the hydrogen binding energy. Outside the exponent, the mass of the hydrogen atom was approximated to equal the mass of the proton in (223). Ignoring helium, $n_{\rm H} = n_{\rm b} - n_{\rm e}$. Taking $n_{\rm b}$ from (217) and expressing (223) in terms of $X_{\rm e}$ results in the Saha equation

$$\frac{1 - X_{\rm e}}{X_{\rm e}^2} = \frac{4\sqrt{2}\zeta(3)}{\sqrt{\pi}} \eta_{\rm B} \left(\frac{T}{m_{\rm e}}\right)^{3/2} e^{B_{\rm H}/T}. \tag{224}$$

The Saha equation (224) describes the equilibrium evolution of free electron fraction $X_{\rm e}$.

As the universe expands, the interactions involved in the recombination reaction (210) become inefficient at keeping the reaction in chemical equilibrium (see e.g. [49]). Then free electron fraction $X_{\rm e}$ no longer obeys the Saha equation (224) and a more general description of its evolution is required.

Tracking the general evolution of $X_{\rm e}$ is slightly more involved than the fairly simple derivation of the Saha equation (224). When solving the Boltzmann equation for electrons, it is necessary to consider which of the recombination reactions (210) contribute to change in $n_{\rm e}$. Forming hydrogen straight into its ground state results in emission of an ionizing photon [50]. Therefore in the relevant reactions hydrogen is formed into an excited state and it later transitions into the ground state. The lifetime of the excited state affects the recombination rate, since the atom can be ionized before it reaches the ground state.

The resulting general equation for $X_{\rm e}$ is called the Peebles equation [50], which in the notation of [42] has the form:

$$X_{\rm e}' = aC\left(\beta(1 - X_{\rm e}) - n_{\rm b}\alpha^{(2)} X_{\rm e}^2\right). \tag{225}$$

Decrease in the free electron fraction by recombination to an excited state is accounted by the second term inside the outer brackets on the right hand side of (225). The recombination rate is [42]

$$\alpha^{(2)} = 9.78 \frac{\alpha^2}{m_{\rm e}^2} \sqrt{\frac{B_{\rm H}}{T}} \ln \frac{B_{\rm H}}{T}. \tag{226}$$

In equation (226), α is the fine structure constant. Increase in $X_{\rm e}$ by ionization of ground state hydrogen atom is described by the first term on the right hand side of (225). The ionization rate is [50]

$$\beta = \left(\frac{m_{\rm e} T}{2\pi}\right)^{3/2} e^{-B_{\rm H}/T} \alpha^{(2)}. \tag{227}$$

Ionization of excited states decreases the rate of change in X_e by factor C. The C factor is the fraction by which the excitation ends in decay, the other option being ionization. Decay of an excited state to the ground state resulting in change of X_e involves either two photon emission at rate $\Lambda_{2\gamma} = 8.227\,\mathrm{s}^{-1}$ [50] or production of Lyman alpha photons at rate [42]

$$\Lambda_\alpha = \frac{(3B_\mathrm{H})^3\mathcal{H}}{(8\pi)^2 a(1-X_\mathrm{e})n_\mathrm{b}}. \tag{228}$$

With excited state ionization rate [42]

$$\beta^{(2)} = \left(\frac{m_\mathrm{e}T}{2\pi}\right)^{3/2} e^{-B_\mathrm{H}/4T}\alpha^{(2)} \tag{229}$$

the C factor has the expression [42]

$$C = \frac{\Lambda_\alpha + \Lambda_{2\gamma}}{\Lambda_\alpha + \Lambda_{2\gamma} + \beta^{(2)}}. \tag{230}$$

5.5 Initial Conditions

To solve the perturbation equations of sections 5.2 – 5.4, initial values must be specified. The quantities whose initial values are determined in this section are the Bardeen potentials Φ and Ψ and the fluid quantities δ_i, v_i and Π_i. For the free electron fraction X_e the initial conditions have already been set, since the non-differential Saha equation (224) can be used as the initial condition for the Peebles equation (225). Since the perspective of this section is to establish initial values for a set of differential equations to be solved, we are referring to the specified period and the corresponding perturbations as "initial" as opposed to the common (see e.g. [35]) nomenclature of labelling them "primordial".

The period of initial conditions was established in section 5.1. That is, we are determining the values of the specified quantities after electrons have become non-relativistic at $T \sim 500\,\mathrm{keV}$, but before scales of interest start entering the horizon at $T \sim 1\,\mathrm{keV}$. Therefore $k \ll \mathcal{H}$ for all scales k. During the initial period the universe is radiation dominated, so that $\rho \approx \rho_\gamma + \rho_\nu$ and $w \approx 1/3$.

The initial conditions are heavily impacted by the level of adiabaticity of the fluid during the initial period. A fluid is adiabatic if its pressure depends solely on energy density, $p = p(\rho)$ (see e.g. [5]). The pressure perturbation in general is therefore

$$\delta p = \frac{\partial p}{\partial \rho}\delta\rho + \delta p_\mathrm{nad}, \tag{231}$$

where δp_nad is the non-adiabatic component of pressure perturbation. With radiation and matter equations of state $p = \rho/3$ and $p = 0$ respectively, the perturbations of a single component fluid are always adiabatic. The non-adiabatic pressure perturbation δp_nad arises from relative differences in density of matter and radiation components

in a mixed fluid. The relative entropy perturbation between fluid components i and j is defined as [51]

$$\begin{aligned} S_{ij} &\equiv -3\mathcal{H}\left(\frac{\delta\rho_i}{\overline{\rho}_i'} - \frac{\delta\rho_j}{\overline{\rho}_j'}\right) \\ &= \frac{\delta_i}{1+w_i} - \frac{\delta_j}{1+w_j}. \end{aligned} \tag{232}$$

The second line in (232) resulted from the background continuity equation (32) and the definition of density contrast (120). With S_{ij} the non-adiabatic pressure perturbation has the expression [51]

$$\delta p_{\rm nad} = \frac{1}{6\mathcal{H}\bar{\rho}'}\sum_{i,j}\bar{\rho}_i'\bar{\rho}_j'(c_i^2 - c_j^2)S_{ij}. \tag{233}$$

In (233) c_i^2 is the speed-of-sound parameter,

$$c_i^2 \equiv \frac{\partial\bar{p}_i}{\partial\bar{\rho}_i}. \tag{234}$$

A non-zero S_{ij} corresponds to a non-adiabatic, or isocurvature mode (see e.g. [35]). For adiabatic perturbations, $S_{ij} = 0$ for all fluid components i and j.

Observations indicate that the initial perturbations are adiabatic [18], so we shall ignore the non-adiabatic pressure perturbation $\delta p_{\rm nad}$. Vanishing relative entropy perturbations (232) then set

$$\delta_{\rm b} = \delta_{\rm c} = \frac{3}{4}\delta_\gamma = \frac{3}{4}\delta_\nu \tag{235}$$

during the initial period.

Adiabatic scalar perturbations have a single degree of freedom. This degree of freedom can be encapsulated by the comoving curvature perturbation $\mathcal{R}$ (see e.g. [52]). In the conformal Newtonian gauge $\mathcal{R}$ has the Fourier space representation[2] (see e.g. [52])

$$\mathcal{R} = \Psi - \mathcal{H}\frac{v}{k}. \tag{236}$$

Taking v/k from one of the Einstein equations (129) results in

$$\mathcal{R} = \Psi + \frac{2}{3}\frac{\mathcal{H}\Phi + \Psi'}{\mathcal{H}(1+w)}. \tag{237}$$

The goal of this determination of initial conditions is to relate the different perturbations to $\mathcal{R}$.

A key feature of the comoving curvature perturbation $\mathcal{R}$ is that it is conserved on superhorion scales [53]. What this implies for the perturbations of the metric is

[2]Note that the extra k compared to the form in [52] results from the Fourier convention specified in section 4.3.

clearest seen in the case of perfect fluid, for which the anisotropic stress Π vanishes. The fourth Einstein equation (131) sets $\Phi = \Psi$ for a perfect fluid. Taking $\mathcal{R}$ to be constant and differentiating (237) gives

$$\mathcal{H}^{-1}\Phi'' + 4\Phi' = 0 \tag{238}$$

in radiation dominance. The Friedmann equations (45) and (46) were used in simplifying (238). The scale factor dependence of the background radiation energy density (35) with the Friedmann equation (45) implies that in radiation dominance

$$\mathcal{H} = \frac{1}{\eta}. \tag{239}$$

With (239), the equation (238) has the general solution

$$\Phi = C_1 + \frac{C_2}{\eta^3}. \tag{240}$$

The terms on the right hand side of (240) are the growing mode and the decaying mode, respectively. After a sufficient time since the generation of the perturbations, the growing has become dominant so that Φ is constant. This result holds also for non-perfect fluids: after the decaying modes have died out, the metric perturbations Φ and Ψ are constant on superhorizon scales for adiabatic perturbations [54, 55].

Thus far we have established that during the initial period $w = 1/3$ due to radiation domination, $k \ll \mathcal{H}$ since scales of interest are superhorizontal, and adiabaticity sets $\delta p = \delta\rho/3$ and $\Phi' = \Psi' = 0$. Inserting these into the Einstein equations (128) – (131) results in

$$\delta = -2\Phi \tag{241}$$

$$v = -\frac{1}{2}\frac{k}{\mathcal{H}}\Phi \tag{242}$$

$$\Pi = \left(\frac{k}{\mathcal{H}}\right)^2 (\Psi - \Phi). \tag{243}$$

With the aforementioned statements and the equation (237), the comoving curvature perturbation becomes

$$\mathcal{R} = \Psi + \frac{1}{2}\Phi. \tag{244}$$

In radiation dominance, $\bar{\rho} \approx \bar{\rho}_\gamma + \bar{\rho}_\nu$ and $\delta\rho \approx \delta\rho_\gamma + \delta\rho_\nu$. With these and (235) we get

$$\delta = \delta_\gamma = \delta_\nu. \tag{245}$$

The equations (235) and (245) relate the initial values of all density contrasts to the initial Bardeen potential Φ through (241).

The derivative δ_i' for non-interacting fluid components was derived in (134). With $\Psi' = 0$ and $\delta p_i = w_i \delta\rho_i$ it becomes

$$\delta_i' = (1 + w_i)kv_i. \tag{246}$$

For photons and baryons an interaction term needs to be added. In general, the derivative of the relative entropy perturbation S_{ij} of (232) is of the form

$$S'_{ij} = k(v_i - v_j) + \text{interactions}. \tag{247}$$

Since S_{ij} remains zero during the initial period, $S'_{\mathrm{ij}} = 0$. For the non-interacting components (247) then implies

$$v_{\mathrm{c}} = v_\nu. \tag{248}$$

In radiation dominance, the number density of photons far outweighs that of baryons, making the interactions insignificant from the photons' perspective. Therefore (247) sets the velocity perturbation of photons equal to the velocity perturbation of dark matter and neutrinos. The baryons are kept tightly bound to photons by scattering, so that $v_{\mathrm{b}} = v_\gamma$. The total velocity perturbation v relates to its components as

$$(\rho + p)v = \sum_i (\rho_i + p_i)v_i. \tag{249}$$

Since all initial component velocity perturbations are equal,

$$v = v_\gamma = v_\nu = v_{\mathrm{c}} = v_{\mathrm{b}}. \tag{250}$$

With equations (242) and (250), the initial velocity perturbations are related to the Bardeen potential Φ.

Well before recombination, photons and baryons were tightly coupled. Interactions with baryons maintained the isotropy of photons, enforcing $\Pi_\gamma = 0$. The whole fluid anisotropic stress divides into component stresses as

$$\bar{p}\Pi = \sum_i \bar{p}_i \Pi_i. \tag{251}$$

With neutrinos being the only component of anisotropic stress,

$$\Pi = f_\nu \Pi_\nu, \tag{252}$$

where f_ν is the neutrino fraction of the radiation energy density in the background

$$f_\nu = \frac{\bar{\rho}_\nu}{\bar{\rho}_\gamma + \bar{\rho}_\nu}. \tag{253}$$

Since the background energy densities of radiation components have the same time dependence (35), f_ν is a constant after electron-positron annihilations. With the parameter values of appendix A, $f_\nu \approx 0.405$.

Similar to photons, interactions with the plasma kept neutrinos isotropic until decoupling, setting all neutrino multipoles from octupole onwards to zero (see e.g. [52]). After decoupling, the higher multipoles start to evolve, but the evolution of multipole l is hindered by the scale dependence in (205) in comparison to the multipole $l - 1$ on superhorizon scales. Therefore during the initial period the $l = 3$

multipole in (204) can be ignored. The equations (204), (242) and (250) relate Π_ν to the Bardeen potential Φ:

$$\Pi_\nu = \frac{2}{5}\left(\frac{k}{\mathcal{H}}\right)^2 \Phi. \tag{254}$$

The Bardeen potentials can now be related to each other by (243), (252) and (254):

$$\Psi = \left(1 + \frac{2}{5} f_\nu\right) \Phi. \tag{255}$$

Substituting this into (244) gives Φ in terms of the comoving curvature perturbation $\mathcal{R}$:

$$\Phi = \frac{10}{15 + 4 f_\nu} \mathcal{R}. \tag{256}$$

With (256) all the initial conditions are related to $\mathcal{R}$ as desired.

6 Solving the Evolution of Perturbations

The evolution of perturbations is now set up by a complete set of differential equations: the four Einstein equations from section 5.2, two equations for both species of matter and Boltzmann hierarchies of the radiation components from sections 5.3 and 5.4 and the Peebles equation for the free electron fraction (225). Two of the Einstein equations can be replaced by continuities $\nabla_\mu G^\mu{}_\nu = 0$ and $\nabla_\mu T^\mu{}_\nu = 0$, leaving two independent equations governing the two metric perturbations Φ and Ψ. The number of equations then matches the number of variables, and with the initial conditions specified in section 5.5, the perturbation equations can be solved.

No exact analytic solution can be found for the complex system of coupled differential equations describing the evolution of the perturbations. Rough solutions can be found by making enough approximations. This is done in section 6.1. Numerical solutions are presented in section 6.2.

6.1 Analytic Approximations

The goal of this section is to derive analytic solutions for the perturbation equations. In particular, we are interested in the behaviour of the density contrast of different fluid components after horizon entry. To get there, a number of approximations need to be made.

The first approximation is to assume the cosmic fluid to be a perfect fluid. For a perfect fluid, the anisotropic stress Π vanishes, as evident from the energy-momentum tensor (15). The fourth Einstein equation (131) then sets $\Psi = \Phi$, leaving the metric (91) with a single perturbation degree of freedom. As discussed when specifying the initial conditions in section 5.5, Thomson scattering keeps the photon distribution isotropic while in radiation domination. Neutrino anisotropies, however, start to develop once the scale enters the horizon as described by the initial period equation (254). Because of this, the following approximate results for radiation describe the behaviour of the neutrinos poorly, as can be seen when comparing them with the numerical solutions in section 6.2.

The second approximation is to treat baryons as completely coupled to photons in radiation dominance and completely decoupled in matter dominance. As baryons are a subdominant component in radiation dominance and we are already ignoring anisotropic stress, we may ignore any effect baryons have on photons in radiation dominance. In effect, the cosmic fluid then consists of radiation and matter with no interactions between them. In radiation dominance, dark matter is the only component behaving as pressureless matter, while in matter dominance baryons behave as matter, too. As the evolution of non-interacting fluid components was established in

section 5.3, the evolution of radiation is described by the neutrino equations (141) and (142) and the evolution of matter by the dark matter equations (143) and (144).

6.1.1 Perturbations in Radiation Dominance

First let us consider radiation perturbations in a radiation dominated universe. With the radiation equation of state $p = \rho/3$ the Einstein equations (128) and (130) become

$$\mathcal{H}^{-1}\Phi' + \Phi + \frac{1}{3}\left(\frac{k}{\mathcal{H}}\right)^2 \Phi = -\frac{1}{2}\delta \tag{257}$$

and

$$\mathcal{H}^{-2}\Phi'' + 3\mathcal{H}^{-1}\Phi' - \Phi = \frac{1}{2}\delta, \tag{258}$$

respectively. Summing these and switching to use the scale factor a as the time variable instead of conformal time yields

$$\frac{d^2\Phi}{da^2} + \left(\frac{a''}{(a')^2} + \frac{4}{a}\right)\frac{d\Phi}{da} + \frac{1}{3}\left(\frac{k}{a'}\right)^2 \Phi = 0. \tag{259}$$

In the equation (35), the energy density of radiation was established to scale as $\rho \propto a^{-4}$. The Friedmann equation (45) then implies that a' is constant and thus $a'' = 0$. With constant a', the equation (259) can further be simplified by using

$$x \equiv \frac{k}{\sqrt{3}\,a'}a = \frac{k}{\sqrt{3}\,\mathcal{H}} \tag{260}$$

as the time variable, resulting in

$$\frac{d^2\Phi}{dx^2} + \frac{4}{x}\frac{d\Phi}{dx} + \Phi = 0. \tag{261}$$

The equation (261) has the general solution

$$\Phi = C_1\frac{x\sin x + \cos x}{x^3} + C_2\frac{\sin x - x\cos x}{x^3}. \tag{262}$$

In section 5.5 it was discussed how the Bardeen potential Φ is constant on superhorizon scales providing that the initial perturbations are adiabatic. Requiring Φ in (262) to stay finite as x approaches 0 sets $C_1 = 0$. The remaining term goes to $C_2/3$ as $x \to 0$, so

$$\Phi = 3\Phi_{\text{in}}\frac{\sin x - x\cos x}{x^3}, \tag{263}$$

where Φ_{in} is the initial value of Φ.

For scales well outside the horizon, $k \ll \mathcal{H}$, or $x \ll 1$. The Bardeen potential Φ then remains constant at its initial value Φ_{in}. The equation (258) then sets the density contrast to a constant value of $\delta_{\text{in}} = -2\Phi_{\text{in}}$, in consistency with (241).

For subhorizontal scales, $x \gg 1$, and Φ evolves as

$$\Phi = -3\Phi_{\text{in}} \frac{\cos x}{x^2}, \tag{264}$$

ie. Φ oscillates with damping. On the left hand side of the equation (257), the term proportional to $k/\mathcal{H}$ dominates, so that

$$\delta = 6\Phi_{\text{in}} \cos x. \tag{265}$$

In this approximation, the density contrast of radiation therefore oscillates with a constant amplitude in radiation dominance. With the coupling between baryons and photons, (265) also implies that the density contrast of baryons oscillates with a constant amplitude.

The equations (143) and (144) describe the evolution of dark matter density contrast and velocity perturbation, respectively. Substituting $\Psi = \Phi$ from (263) into them yields

$$\delta_{\text{c}}' = kv_{\text{c}} + 3\Phi' \tag{266}$$
$$v_{\text{c}}' = -\mathcal{H}v_{\text{c}} - k\Phi. \tag{267}$$

Differentiating (266) and performing substitutions with (267) results in a second order differential equation for δ_{c}:

$$\delta_{\text{c}}'' + \mathcal{H}\delta_{\text{c}}' = 3\Phi'' + 3\mathcal{H}\Phi' - k^2\Phi. \tag{268}$$

With x from (260) as the time variable the equation (268) becomes

$$\frac{d^2\delta_{\text{c}}}{dx^2} + \frac{1}{x}\frac{d\delta_{\text{c}}}{dx} = 3\frac{d^2\Phi}{dx^2} + \frac{3}{x}\frac{d\Phi}{dx} - 3\Phi. \tag{269}$$

In (269), the right hand side acts as a source to the evolution of δ_{c}, let us denote it by S:

$$S(x) \equiv 3\frac{d^2\Phi}{dx^2} + \frac{3}{x}\frac{d\Phi}{dx} - 3\Phi. \tag{270}$$

An explicit form for S can be obtained from (263).

Setting the source term S to zero, one obtains a homogeneous solution to the equation (269):

$$\delta_{\text{c,homog}} = C_1 + C_2 \ln x. \tag{271}$$

A general solution can be acquired by variation of parameters and has the form

$$\delta_{\text{c}} = C_1 + C_2 \ln x + \int_0^x dx'\, x' S(x')(\ln x - \ln x'). \tag{272}$$

As x approaches zero, the intergral in (272) goes to zero. Following results from section 5.5, we require δ_{c} to stay finite at the limit $x \to 0$. Therefore $C_2 = 0$ and C_1 is the initial value of δ_{c}.

In the subhorizon limit $x \gg 1$, Φ approaches zero, as seen in equation (264). Therefore the source term S goes to zero as well, and we can do an approximation where the integral in (272) goes to infinity:

$$\delta_{\mathrm{c}} = \delta_{\mathrm{c,in}} + \int_0^\infty dx'\, x' S(x')(\ln x - \ln x'). \tag{273}$$

Now only the first term in the integral has x dependence, so that δ_{c} is of the form

$$\delta_{\mathrm{c}} = A_1 + A_2 \ln x \tag{274}$$

with constants A_1 and A_2. As a' is constant in radiation dominance, $x \propto a$ as per the definition of x (260). Hence in radiation dominance dark matter starts accumulating logarithmically with respect to the scale factor a.

6.1.2 Perturbations in Matter Dominance

In matter dominance, the cosmic fluid is approximatively pressureless: $p \approx 0$. The Einstein equation (130) for a perfect fluid then reads

$$\Phi'' + 3\mathcal{H}\Phi' = 0. \tag{275}$$

With the scale factor a as the time variable, the equation (275) becomes

$$\frac{d^2\Phi}{da^2} + \left(\frac{a''}{(a')^2} + \frac{3}{a}\right)\frac{d\Phi}{da} = 0. \tag{276}$$

The Friedmann equations (45) and (46) for $p = 0$ result in a differential equation for the scale factor:

$$\frac{a''}{(a')^2} = \frac{1}{2a}. \tag{277}$$

Substituting this into (276) yields a closed equation for Φ:

$$\frac{d^2\Phi}{da^2} + \frac{7}{2a}\frac{d\Phi}{da} = 0. \tag{278}$$

The equation (278) has the general solution

$$\Phi = \frac{C_1}{a^{5/2}} + C_2. \tag{279}$$

The first term on the right hand side of (279) is a decaying term due to the scale factor growing with time. For sufficiently late times the decaying term can be ignored, resulting in the potential Φ remaining constant.

Density contrast δ can be related to the metric perturbation Φ with the first Einstein equation (128):

$$\delta = -2\left(1 + \frac{1}{3}\left(\frac{k}{\mathcal{H}}\right)^2\right)\Phi. \tag{280}$$

On subhorizon scales, the term proportional to $k/\mathcal{H}$ dominates:

$$\delta \approx -\frac{2}{3}\left(\frac{k}{\mathcal{H}}\right)^2 \Phi. \tag{281}$$

According to (34) the energy density of matter scales as $\rho \propto a^{-3}$. This scaling with the Friedmann equation (45) results in $\mathcal{H}^2 \propto a^{-1}$. Therefore, with the decaying mode of Φ in (279) died out, the equation (281) has the matter density contrast grow linearly with a on subhorizon scales:

$$\delta \propto a. \tag{282}$$

The density contrast δ of both matter components, baryons and dark matter, therefore grow linearly in matter dominance.

Comparing (282) with the equation (274) we see that the accumulation of dark matter becomes more rapid as the universe transitions from radiation dominance to matter dominance. Baryons on the other hand are prevented from accumulation in radiation dominance and start forming structures only in matter dominance. The overdensities that the dark matter has formed by the time the universe becomes matter dominated act as gravity wells into which baryonic matter is pulled.

6.2 Numerical Solutions

This section presents numerical solutions to the perturbation equations specified in section 5. The Python code that was used to compute the solutions can be found in the appendix B and at `http://users.jyu.fi/~tuereiaa/structform/realFluid.py`. The values of cosmological parameters used in the computation are listed in appendix A.

When specifying the initial conditions in 5.5, the initial values of perturbations were related to the initial comoving curvature perturbation $\mathcal{R}_{\text{in}}$. As a result, the numerical solutions are computed in units of $\mathcal{R}_{\text{in}}$. In other words, the computed solution for the evolution of quantity q is its transfer function T_q, defined by (see e.g. [35])

$$q(k,t) \equiv T_q(k,t)\mathcal{R}_{\text{in}}(k). \tag{283}$$

The transfer function encaptures the time dependence of the quantity q. Alternative definitions for the transfer function usually add a constant factor to the right hand side of (283) to set the initial value of the transfer function to unity (see e.g. [35]).

In the presented solutions, the Boltzmann hierarchies of photons and neutrinos are truncated at the multipole $l_{\text{max}} = 2$. The multipole $l_{\text{max}} + 1$ of the brightness function is approximated by (203) both for photons and neutrinos. The solutions are therefore a slight improvement over the ideal fluid approximation, for which $l_{\text{max}} = 1$ and $(\Theta_{\gamma/\nu})_l = 0$ for all $l \geq 2$. The used l_{max} is still relatively low; for numerical computations with a similar approach and l_{max} in the order of thousands, see e.g. [42].

The equations of section 5 use the conformal time η as the time variable. To make the solutions independent of the scaling of the scale factor, the numerical solutions use redshift z from (29) as the time variable in the form

$$\frac{1}{1+z} = \frac{a}{a_0}. \tag{284}$$

The inverse is taken so that the time variable would grow with time.

In the solutions, a specific comoving scale k is referred to by the corresponding present day physical $k_{\mathrm{phys}}(t_0)$. With the relation (96) we define

$$k_0 \equiv k_{\mathrm{phys}}(t_0) = \frac{k}{a_0}. \tag{285}$$

6.2.1 Matter Perturbations

Numerical solutions for the density contrast of dark matter on four scales k_0 are shown in figure 2a. The figure shows that dark matter perturbations start to grow right after horizon entry. This is expected, since dark matter is affected only by gravitation, which causes the accumulation. For scales that enter the horizon during the radiation dominated epoch, the rate of accumulation decreases until matter dominance is reached. In matter dominance, the growth of the density perturbation is approximately linear in a.

The numerical results of figure 2a agree well with the analytical approximations of section 6.1. The decelerating growth of the dark matter density perturbation during radiation dominance can be identified as logarithmic in a with the equation (274), and the linear growth in matter dominance was seen in equation (282).

As can be seen from the figure 2b, the evolution of baryon density contrast in radiation dominance is significantly different from that of dark matter. In radiation dominance, the coupling of baryons to photons with the latter being a dominant fluid component forces baryons to follow the behaviour of photons. The density contrast of photons in figure 3a shows similar oscillations during the radiation dominated epoch as the baryon density contrast.

After the universe has entered matter dominance, the coupling between baryons and photons is broken and baryonic matter is free to evolve similar to dark matter. The analytic approximation of $\delta_{\mathrm{b}} \propto a$ from equation (282) agrees well with the numerical solution of figure 2b in matter dominance. Since dark matter has started to accumulate earlier during the radiation dominated epoch, it has created gravity wells before baryonic matter starts to accumulate. As a result, baryonic matter will gather into overdensities of dark matter.

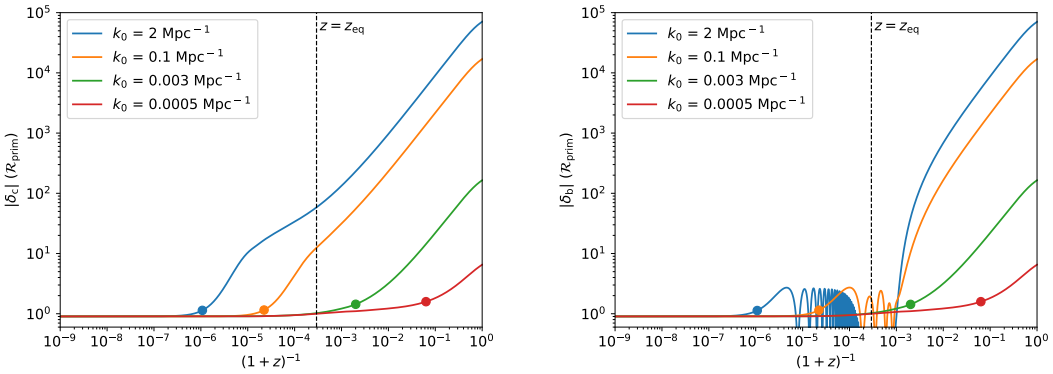

(a) CDM **(b)** Baryons

Figure 2. Numerically solved transfer functions of dark matter and baryon density contrasts on four different scales. Matter-radiation equilibrium is denoted by a vertical line. The dots on the curves represent the approximate point of horizon entry, where $k = aH$. The shown values of the scales correspond to their present day physical values, $k_0 = k/a_0$.

6.2.2 Radiation Perturbations

Numerical solutions for the density contrast of radiation components are shown in figures 3a and 3b. Unlike matter components, the radiation components do not accumulate: for radiation, the gravitational pull is countered by pressure, resulting in oscillatory behaviour visible in the figures.

In the approximative equation of (265), radiation was found to oscillate with a constant amplitude in radiation dominance. In the numerical solutions of figures 3a and 3b, this holds only for photons. This is because the perfect fluid approximation is more valid for photons in radiation dominance than for neutrinos. The validity of perfect fluid approximation can be seen from figures 4a and 4b where numerical solutions for the anisotropic stresses of the radiation components are plotted. The smaller the anisotropic stress is, the better the fluid is described by the perfect fluid model. Photons start to gain anisotropic stress only after matter-radiation equilibrium, whereas neutrinos start to deviate from the perfect fluid approximation right after horizon entry.

In the Boltzmann hierarchy of photons (196) – (199), the differential equation for the multipole l of the brightness function involves multipoles $l-1$ and $l+1$. Since the $l = 2$ multipole corresponding to the anisotropic stress as per equation (189) vanishes for photons in radiation dominance, the equations for the density contrast δ_γ and velocity perturbation v_γ are decoupled from the higher multipoles. The low truncation value of $l_{\text{max}} = 2$ therefore affects photons in radiation dominance only indirectly through the impact neutrinos have on the metric.

The numerical solutions for neutrinos are less reliable for all periods after horizon entry. With non-zero anisotropic stress, all multipoles have in principle an effect on the density perturbation. The truncation scheme of (203) relies on the sum of the

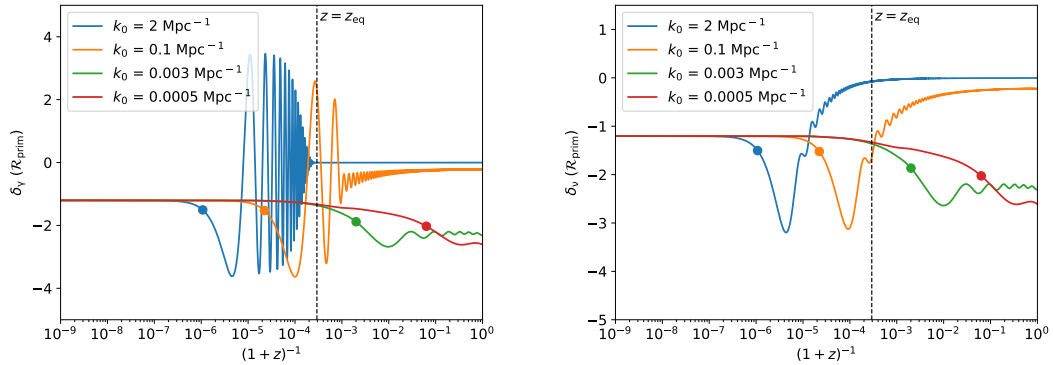

(a) Photons **(b)** Neutrinos

Figure 3. Numerically solved transfer functions of photon and neutrino density contrasts on four different scales. Matter-radiation equilibrium is denoted by a vertical line. The dots on the curves represent the approximate point of horizon entry, where $k = aH$. The shown values of the scales correspond to their present day physical values, $k_0 = k/a_0$.

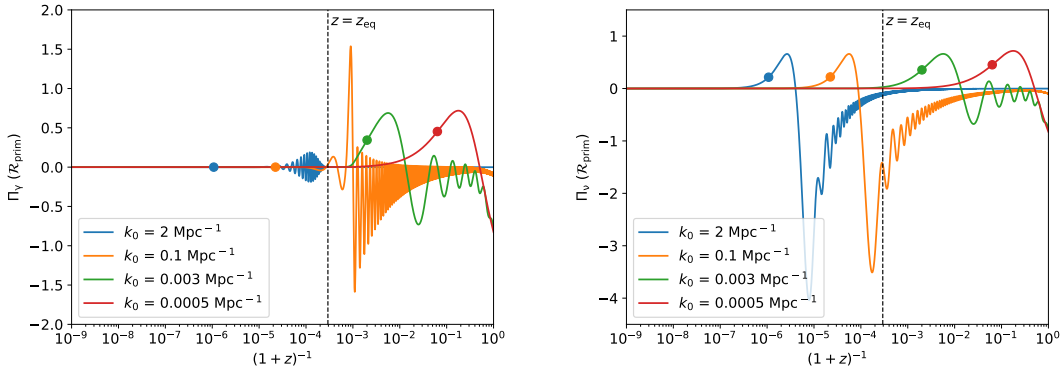

(a) Photons **(b)** Neutrinos

Figure 4. Numerically solved transfer functions of anisotropic stress of the radiation components on four different scales. Matter-radiation equilibrium is denoted by a vertical line. The dots on the curves represent the approximate point of horizon entry, where $k = aH$. The shown values of the scales correspond to their present day physical values, $k_0 = k/a_0$.

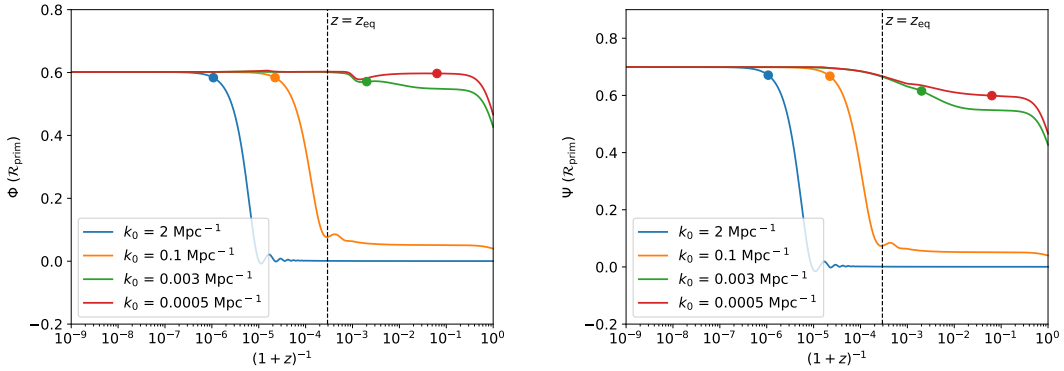

(a) Φ **(b)** Ψ

Figure 5. Numerically solved transfer functions of the Bardeen potentials on four different scales. Matter-radiation equilibrium is denoted by a vertical line. The dots on the curves represent the approximate point of horizon entry, where $k = aH$. The shown values of the scales correspond to their present day physical values, $k_0 = k/a_0$.

Bardeen potentials Φ and Ψ remaining relatively unchanged. This is an especially ill-justified approximation in radiation dominance, as can be seen from the figures 5a and 5b.

6.2.3 Metric Perturbations

Figures 5a and 5b depict numerical solutions for the Bardeen potentials Φ and Ψ, respectively. The potentials behave similarly after horizon entry, only having different initial values. Both decay in radiation dominance and remain constant in matter dominance. Comparing the figures with the approximative analytic results of (264) and (279) we can see that both methods predicted similar behaviours for the Bardeen potentials with the analytic approximations missing the difference between Φ and Ψ.

The drop in the potentials starting at $z \approx 3$ is because of the emergence of the vacuum energy dominated epoch: as a homogeneous and isotropic fluid component becomes dominant, the metric approaches Robertson-Walker form and hence its perturbations start to vanish.

7 End of the Linear Regime

The perturbation theory approach to the structure formation is valid only for as long as the perturbations are small. Since the formation of cosmic structure sees matter perturbations grow, at some point the matter density contrast δ_{m} on a given scale reaches unity. At that point, $\bar{\rho}_{\mathrm{m}} = \delta\rho_{\mathrm{m}}$, and the assumption of small perturbations has been well invalidated on that scale.

An analytic estimate for the validity of the perturbation theory is the subject of this section. Here we shall present what is called the spherical collapse model of structure formation [10]. In the model, a spherically symmetric overdensity of matter collapses under its own gravity. Comparing the growth of matter density contrast in the spherical collapse model with that of linear perturbation theory gives a sense of when and how the linear theory prediction of structure formation begins to fail.

Because of the assumption of spherical symmetry, the spherical collapse model pertains to a perturbation of a particular and idealized geometry. The quantitative deviation between the linear model and the spherical collapse model found in the following comparison is a precise measure on the failure of the linear theory only for that special case. Still, the spherical collapse model provides a rule-of-thumb for the point at which the evolution of matter perturbations becomes non-linear (see e.g. [29]).

The linear perturbation theory is the simplest form of a perturbation theory. A higher order perturbation theory [8, 9] is a more precise description of the evolution of perturbations at the cost of computational complexity as well as introducing phenomena absent from the linear theory, such as mixing of scalar, vector and tensor perturbations. However, the benefits of a higher order theory are limited because expanding a quantity to any finite order in perturbation becomes invalid at the point when the perturbation reaches the background value. Beyond the linear regime, N-body simulations [11–13] can be utilized in analyzing the evolution of perturbations.

7.1 The Spherical Collapse Model

The spherical collapse model describes the collapse of a spherically symmetric matter overdensity under gravity. The overdense region is assumed to be homogeneous and isotropic so that it can be modelled as a closed FRW universe embedded in a flat background FRW universe.

As seen in section 6.2, baryons start to accumulate only after the universe has entered matter dominance, and the rate of dark matter accumulation increases significantly after matter-radiation equilibrium. It is a decent approximation to

restrict ourselves in the matter-dominated universe when gauging the end of the applicability of the linear theory.

As the background universe has no spatial curvature, its energy density $\bar{\rho}$ equals the background critical density $\bar{\rho}_\mathrm{c}$ (38):

$$\bar{\rho} = \bar{\rho}_\mathrm{c} \equiv 3M_\mathrm{p}^2 \bar{H}^2. \tag{286}$$

Since the inspected region is overdense, its energy density ρ exceeds the critical energy density of the region ρ_c. By the definition of the density parameter Ω (37), the region has $\Omega > 1$ and, with the Friedmann equation (26), curvature parameter $K > 0$.

Let us denote by t_* some initial time when the density parameter of the overdense region Ω is still close to unity. As the curvature parameter K is a constant, with the Friedmann equation (26) and the density parameter (37) it can be expressed as

$$K = H_*^2 a_*^2 (\Omega_* - 1). \tag{287}$$

In matter dominance, the energy density scales as $\rho \propto a^{-3}$ as described in (34). With this scaling the energy density of the region has the expression

$$\rho = \rho_* \left(\frac{a_*}{a} \right)^3. \tag{288}$$

Using (288) with the Friedmann equation (26) and the definition of the density parameter (37) we then get

$$\frac{da}{dt} = H_* a_* \sqrt{\Omega_* - 1} \sqrt{\frac{C - a}{a}}, \tag{289}$$

where

$$C \equiv \frac{\Omega_* a_*}{\Omega_* - 1}. \tag{290}$$

Because the region is collapsing, its scale factor is between zero and some maximum value a_max. As such, the solution of the equation (289) can be parametrized by the development angle θ:

$$a(\theta) \equiv C \sin^2 \frac{\theta}{2} = \frac{1}{2} C (1 - \cos\theta). \tag{291}$$

Substituting this back into (289) yields

$$\frac{dt}{d\theta} = \frac{\Omega_*}{2H_*(\Omega_* - 1)^{3/2}} (1 - \cos\theta). \tag{292}$$

The coordinate time in terms of the development angle is then

$$t(\theta) = \frac{\Omega_*}{2H_*(\Omega_* - 1)^{3/2}} (\theta - \sin\theta). \tag{293}$$

Using (287), (288) and (291) with the Friedmann equation (26) gives the energy density of the overdense region in terms of the development angle θ and the Hubble rate H of the region:

$$\rho = \frac{6M_{\mathrm{p}}^2 H^2}{1+\cos\theta}. \tag{294}$$

The equations (286) and (294) give an expression for the density contrast $\delta = (\rho - \bar{\rho})/\bar{\rho}$ of the overdense region:

$$\delta = \frac{2}{1+\cos\theta}\left(\frac{H}{\bar{H}}\right)^2 - 1. \tag{295}$$

The Hubble rate of the overdense region in terms of the development angle can be computed with (291) and (292):

$$H = \frac{\dot{a}}{a} = \frac{2H_*(\Omega_* - 1)^{3/2}}{\Omega_*}\frac{\sin\theta}{(1-\cos\theta)^2}. \tag{296}$$

In the background, the Friedmann equation (26) with the matter dominance energy density (34) is

$$\bar{H}^2 = \left(\frac{\dot{\bar{a}}}{\bar{a}}\right)^2 = \frac{\bar{\rho}_0}{3M_{\mathrm{p}}^2}\left(\frac{\bar{a}_0}{\bar{a}}\right)^3. \tag{297}$$

Solving the scale factor from the equation (297) results in $\bar{a} \propto t^{2/3}$. The Hubble rate in the background universe is then

$$\bar{H} = \frac{2}{3t}. \tag{298}$$

The coordinate time t is the same for both the overdense region and the background. Substituting t in the equation (298) with (293) results in

$$\bar{H} = \frac{4H_*(\Omega_* - 1)^{3/2}}{3\Omega_*}\frac{1}{\theta - \sin\theta}. \tag{299}$$

Substituting the Hubble rates of (296) and (299) into (295), the density contrast of the overdense region is

$$\delta = \frac{9}{2}\frac{(\theta - \sin\theta)^2}{(1-\cos\theta)^3} - 1. \tag{300}$$

As the development angle θ approaches 2π, the scale factor a goes to zero and the density contrast δ to infinity as per equations (291) and (300), respectively. Nothing prevents a perfectly spherical cloud of pressureless matter from collapsing under its own gravity to an infinitely small region, which leads to an infinite density contrast. Evidently matter can and does collapse into structures other than black holes, resulting in finite density contrasts. Hence the spherical collapse model for pressureless fluid has a limited range of validity in description of a realistic collapse process, and it overestimates the growth of perturbations.

At the other limit of $\theta \to 0$, the inspected region assimilates to the flat background with the density contrast going to zero.

7.2 Comparison with the Linear Theory

Next we shall see how the spherical collapse model prediction for the density contrast expressed in the equation (300) deviates from the prediction given by the linear perturbation theory. As was done with the spherical collapse model, matter is approximated to be pressureless and free of interactions, ie. the fluid is predominantly composed of cold dark matter.

As seen in (282), the linear theory prediction for the density contrast δ^{lin} is proportional to the scale factor a in matter dominance. Since $a \propto t^{2/3}$ in matter dominance,

$$\delta^{\text{lin}} = \delta_*^{\text{lin}} \left(\frac{t}{t_*} \right)^{2/3} . \tag{301}$$

Expressing t in terms of the development angle θ with (293) yields

$$\delta^{\text{lin}} = \delta_*^{\text{lin}} \left(\frac{\theta - \sin\theta}{\theta_* - \sin\theta_*} \right)^{2/3} . \tag{302}$$

Taking the time t_* to again be early from the perspective of the collapse, we have $\delta_*^{\text{lin}} \approx \delta_*$. Taking δ_* from (300)

$$\delta^{\text{lin}} = \left(\frac{9}{2} \frac{(\theta_* - \sin\theta_*)^2}{(1 - \cos\theta_*)^3} - 1 \right) \left(\frac{\theta - \sin\theta}{\theta_* - \sin\theta_*} \right)^{2/3} . \tag{303}$$

At the limit $\theta_* \to 0$, the equation (303) becomes

$$\delta^{\text{lin}} = \frac{3}{5} \left(\frac{3(\theta - \sin\theta)}{4} \right)^{2/3} . \tag{304}$$

The density contrasts both from the spherical collapse model δ and from the linear perturbation theory δ^{lin} are plotted in the figure 6 as functions of the development angle θ. Since the linear theory is only valid for small perturbations by construction, the density contrasts start to deviate at $\delta \approx 1$. The linear theory is inable to describe the collapse of matter with the density contrast reaching the well-known value (see e.g. [56])

$$\begin{aligned} \delta^{\text{lin}}(\theta = 2\pi) &= \frac{3}{5} \left(\frac{3\pi}{2} \right)^{2/3} \\ &\approx 1.686 \end{aligned} \tag{305}$$

at the time of the collapse. The linear theory therefore underestimates the growth of spherical perturbations. By the time the linear theory value for the density contrast has reached approximately 1.7, spherical perturbations have undergone complete collapse.

A notable application of the linear theory density contrast at the time of the collapse (305) can be found in the Press-Schechter formalism [57]. The Press-Schechter formalism can be used to predict the abundance of gravitationally bound large scale objects, such as galaxy clusters. The bound objects are identified by their density contrast exceeding a critical value, which can be taken to be the spherical collapse value of (305) (see e.g. [56]).

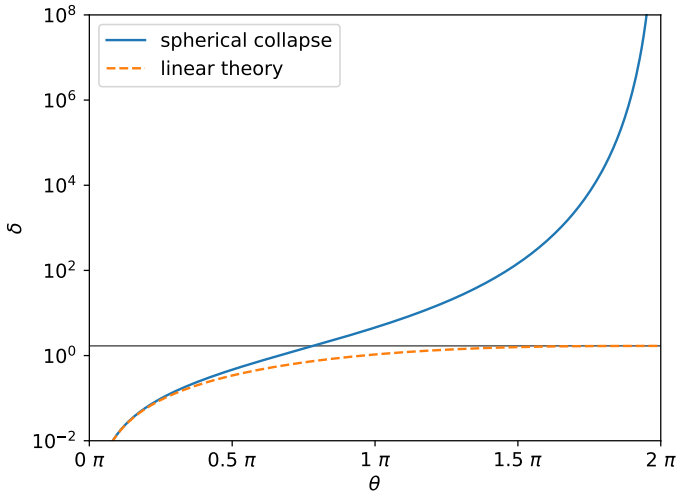

Figure 6. The density contrast δ both from the spherical collapse model and the linear perturbation theory as functions of the development angle θ from equations (300) and (304), respectively. The graphs start to deviate at $\delta \approx 1$, when the linear theory becomes invalid. At collapse time $\theta = 2\pi$, the linear theory prediction reaches $\delta \approx 1.686$ (the horizontal line in the figure), whereas the spherical collapse prediction goes to infinity.

8 Conclusions

The study of cosmological perturbations remains a key topic in cosmology. In the past few decades, much of the observational focus in cosmology has been on investigating the temperature anisotropies in the cosmic microwave background [24, 58, 59]. With the upcoming galaxy surveys [60–62], the focus of observations is shifting from the early universe as imprinted on the CMB to more recent history of the universe, where structure has been forming over the course of billions of years.

In this thesis, we have reviewed the evolution of cosmic scalar perturbations within the context of linear perturbation theory. At the core of this review is the presentation of the derivation of the evolution equations for the perturbations in section 5. In the set of derived equations, there are four Einstein equations (128) – (131). These are the equations of the metric perturbations Φ and Ψ. The extra two equations are there because of the continuity properties $\nabla_\mu G^{\mu\nu} = 0$ and $\nabla_\mu T^{\mu\nu} = 0$.

For matter components, there are equations for the density contrast δ and the velocity perturbation v. The density contrast equation for baryonic matter (206) is identical to that of dark matter (143), reflecting the fact that the low energy scatterings between photons and baryons transfer very little energy. The velocity perturbation equations differ by the baryon equation (209) containing an extra term compared to the dark matter equation (144) as baryons exchange momentum with the photons.

The evolution of the radiation components is governed by their respective Boltzmann hierarchies. A Boltzmann hierarchy constitutes of an infinite series of coupled differential equations, each describing the evolution of a multipole of the brightness function. Similar to matter components, the photon hierarchy (196) – (199) differs from the neutrino hierarchy (141), (142), (204), (205) by the inclusion of interaction terms.

A major choice made in the derivation of evolution equations was to keep perturbations only up to linear order. The linear perturbation theory is the simplest choice for analyzing the structure formation. The evolution equations have been derived up to second order in perturbations [8, 9], but the complexity of the theory is significantly increased in the process. One of the virtues of the linear perturbation theory is that it allows the restriction to only scalar perturbations as they do not couple with vector and tensor perturbations in the linear order. The gains of going to a higher order perturbation theory are also limited by the fact that a perturbative approach of any order becomes invalid when perturbations reach background values.

Section 6 presents solutions to the evolution equations. The evolution of matter density contrasts in figure 2 shows that the structure formation begins with the dark matter starting to accumulate in radiation dominance. Baryonic matter is prevented from accumulation until decoupling from photons around redshift $z \approx 1000$. Figure 3

shows that the density contrasts of the radiation components oscillate, as gravity and pressure counteract each other.

By comparing the analytic approximations of section 6.1 with the numerical solutions of section 6.2 one can see how ignoring the interactions between photons and baryons and using the perfect fluid approximation affects the predicted evolution of perturbations. The analytic approximations yield heuristics similar to those of the numerical solutions. The logarithmic growth of dark matter density contrast in radiation dominance described by the equation (274) is reflected in the numerical solution of figure 2a. Numerical solutions for both baryonic and dark matter density contrasts in figures 2a and 2b show the linear growth in terms of the scale factor in matter dominance predicted by the equation (282). The constant amplitude oscillation of radiation density contrast in radiation dominance in equation (265) is seen with photons in figure 3a. For neutrinos, the approximate treatment is more erraneous, as the numerical solution of figure 3b shows damped oscillations.

In the numerical solutions of section 6.2, the Boltzmann hierarchies of photons and neutrinos were chosen to be truncated at multipole $l = 2$, with the multipole $l = 3$ approximated by (203). A low truncation limit reduces the accuracy of the numerical solutions. The results for photons in radiation dominance are of fair accuracy due to vanishing of the multipole $l = 2$, corresponding to anisotropic stress, as seen in figure (4a). For neutrinos at all times and for photons in matter dominance the numerical solutions are to be taken as rudimentary.

The failing of the linear perturbation theory is examined in section 7. Figure 6 compares the approximated density contrast in matter dominance from the linear theory to that given by the spherical collapse model. From the figure we see that the linear theory underestimates the density contrast after the contrast has grown to unity. The spherical collapse model also provides a way to identify collapsed structures from linear analysis by the critical density contrast of $\delta \approx 1.7$ given by the equation (305).

References

[1] M. Einasto et al. “SDSS DR7 Superclusters”. In: *Astronomy & Astrophysics* 535 (2011). DOI: 10.1051/0004-6361/201117529.

[2] E. Tempel et al. “Detecting Filamentary Pattern in the Cosmic Web: A Catalogue of Filaments for the SDSS”. In: *Monthly Notices of the Royal Astronomical Society* 438 (2013). DOI: 10.1093/mnras/stt2454.

[3] E. M. Lifshitz. “On the Gravitational Stability of the Expanding Universe”. In: *Journal of Physics (USSR)* 10 (1946), pp. 116–129. DOI: 10.1007/s10714-016-2165-8.

[4] H. Kodama and M. Sasaki. “Cosmological Perturbation Theory”. In: *Progress of Theoretical Physics Supplement* 78 (1984), pp. 1–166. DOI: 10.1143/PTPS.78.1.

[5] V. F. Mukhanov, H. Feldman, and R. Brandenberger. “Theory of Cosmological Perturbations”. In: *Physics Reports* 215 (1992), pp. 203–333. DOI: 10.1016/0370-1573(92)90044-Z.

[6] P. J. E. Peebles. “The Black-Body Radiation Content of the Universe and the Formation of Galaxies”. In: *The Astrophysical Journal* 142 (1965), p. 1317. DOI: 10.1086/148417.

[7] P. J. E. Peebles and J. T. Yu. “Primeval Adiabatic Perturbation in an Expanding Universe”. In: *The Astrophysical Journal* 162 (1970), p. 815. DOI: 10.1086/150713.

[8] H. Noh and J.-C. Hwang. “Second-Order Perturbations of the Friedmann World Model”. In: *Physical Review D* 69 (2004), p. 104011. DOI: 10.1103/PhysRevD.69.104011.

[9] K. Nakamura. “Second-Order Gauge Invariant Cosmological Perturbation Theory. Einstein Equations in Terms of Gauge Invariant Variables”. In: *Progress of Theoretical Physics* 117 (2007), pp. 17–74. DOI: 10.1143/PTP.117.17.

[10] J. E. Gunn and J. R. Gott III. “On the Infall of Matter Into Clusters of Galaxies and Some Effects on Their Evolution”. In: *The Astrophysical Journal* 176 (1972), pp. 1–20. DOI: 10.1086/151605.

[11] M. Boylan-Kolchin et al. “Resolving Cosmic Structure Formation with the Millennium-II Simulation”. In: *Monthly Notices of the Royal Astronomical Society* 398.3 (2009), pp. 1150–1164. DOI: 10.1111/j.1365-2966.2009.15191.x.

[12] A. A. Klypin, S. Trujillo-Gomez, and J. Primack. "Dark Matter Halos in the Standard Cosmological Model: Results from the Bolshoi Simulation". In: *The Astrophysical Journal* 740.2 (2011), p. 102. DOI: 10.1088/0004-637x/740/2/102.

[13] R. E. Angulo et al. "Scaling Relations for Galaxy Clusters in the Millennium-XXL Simulation". In: *Monthly Notices of the Royal Astronomical Society* 426.3 (2012), pp. 2046–2062. DOI: 10.1111/j.1365-2966.2012.21830.x.

[14] A. H. Guth. "Inflationary Universe: A Possible Solution to the Horizon and Flatness Problems". In: *Physical Review D* 23 (1981), pp. 347–356. DOI: 10.1103/PhysRevD.23.347.

[15] A. D. Linde. "A New Inflationary Universe Scenario: A Possible Solution of the Horizon, Flatness, Homogeneity, Isotropy and Primordial Monopole Problems". In: *Physics Letters* 108B (1982), pp. 389–393. DOI: 10.1016/0370-2693(82)91219-9.

[16] A. Albrecht and P. J. Steinhardt. "Cosmology for Grand Unified Theories with Radiatively Induced Symmetry Breaking". In: *Physical Review Letters* 48 (1982), pp. 1220–1223. DOI: 10.1103/PhysRevLett.48.1220.

[17] J. M. Bardeen, P. J. Steinhardt, and M. S. Turner. "Spontaneous Creation of Almost Scale-Free Density Perturbations in an Inflationary Universe". In: *Physical Review D* 28 (1983), pp. 679–693. DOI: 10.1103/PhysRevD.28.679.

[18] Planck Collaboration. "Planck 2015 results. XIII. Cosmological Parameters". In: *Astronomy & Astrophysics* 594 (2016), A13. DOI: 10.1051/0004-6361/201525830.

[19] C. M. Will. "The Confrontation between General Relativity and Experiment". In: *Living Reviews in Relativity* 17.1 (2014), p. 4. DOI: 10.12942/lrr-2014-4.

[20] LIGO Scientific Collaboration and Virgo Collaboration. "Observation of Gravitational Waves from a Binary Black Hole Merger". In: *Physical Review Letters* 116 (6 2016), p. 061102. DOI: 10.1103/PhysRevLett.116.061102.

[21] S. M. Carroll. *Spacetime and Geometry. An Introduction to General Relativity.* Addison Wesley, 2004.

[22] Planck Collaboration. "Planck 2015 results. XVI. Isotropy and Statistics of the CMB". In: *Astronomy Astrophysics* 594 (2016), A16. DOI: 10.1051/0004-6361/201526681.

[23] P. Sarkar et al. "The Scale of Homogeneity of the Galaxy Distribution in SDSS DR6". In: *Monthly Notices of the Royal Astronomical Society: Letters* 399 (2009), pp. L128–L131. DOI: 10.1111/j.1745-3933.2009.00738.x.

[24] Planck Collaboration. "Planck 2018 results. I. Overview and the cosmological legacy of Planck". In: *arXiv e-prints*, arXiv:1807.06205 (), arXiv:1807.06205. arXiv: 1807.06205 [astro-ph.CO].

[25] P. J. E. Peebles. *The Large-Scale Structure of the Universe*. Princeton University Press, 1980.

[26] J. M. Bardeen. "Gauge-Invariant Cosmological Perturbations". In: *Physical Review D* 22 (1980), pp. 1882–1905. DOI: 10.1103/PhysRevD.22.1882.

[27] J. M. Stewart. "Perturbations of Friedmann-Robertson-Walker Cosmological Models". In: *Classical and Quantum Gravity* 7 (1990), pp. 1169–1180. DOI: 10.1088/0264-9381/7/7/013.

[28] S. Shen et al. "The Size Distribution of Galaxies in the Sloan Digital Sky Survey". In: *Monthly Notices of the Royal Astronomical Society* 343 (2003), pp. 978–994. DOI: 10.1046/j.1365-8711.2003.06740.x.

[29] S. Dodelson. *Modern Cosmology*. Academic Press, 2003.

[30] E. W. Kolb and M. Turner. *The Early Universe*. Frontiers In Physics. Westview Press, 1994.

[31] D. J. Fixsen. "The Temperature of the Cosmic Microwave Background". In: *The Astrophysical Journal* 707 (2009), pp. 916–920. DOI: 10.1088/0004-637X/707/2/916.

[32] G. B. Rybicki and A. P. Lightman. *Radiative Processes in Astrophysics*. Wiley, 1979.

[33] M. Le Bellac, F. Mortessagne, and G. G. Batrouni. *Equilibrium and Non-Equilibrium Statistical Thermodynamics*. Cambridge University Press, 2004.

[34] S. de Groot, W. A. van Leeuwen, and C. G. van Weert. *Relativistic Kinetic Theory. Principles and Applications*. North-Holland Publishing Company, 1980.

[35] D. H. Lyth and A. R. Liddle. *The Primordial Density Perturbation. Cosmology, Inflation and the Origin of Structure*. Cambridge University Press, 2009.

[36] D. Fixsen et al. "The Cosmic Microwave Background Spectrum from the Full COBE/FIRAS Data Set". In: *The Astrophysical Journal* 473 (1996), pp. 576–587. DOI: 10.1086/178173.

[37] Planck Collaboration. "Planck 2015 results. I. Overview of Products and Scientific Results". In: *Astronomy & Astrophysics* 594 (2016), A1. DOI: 10.1051/0004-6361/201527101.

[38] J. Chluba and R. A. Sunyaev. "The Evolution of CMB Spectral Distortions in the Early Universe". In: *Monthly Notices of the Royal Astronomical Society* 419.2 (2012), pp. 1294–1314. DOI: 10.1111/j.1365-2966.2011.19786.x.

[39] Y. B. Zeldovich and R. A. Sunyaev. "The Interaction of Matter and Radiation in a Hot-Model Universe". In: *Astrophysics and Space Science* 4 (1969), pp. 301–316. DOI: 10.1007/BF00661821.

[40] A. F. Illarionov and R. A. Sunyaev. "Comptonization, Characteristic Radiation Spectra, and Thermal Balance of Low-Density Plasma". In: *Soviet Astronomy* 18 (1975), pp. 413–419.

[41] L. Danese and G. de Zotti. "Double Compton Process and the Spectrum of the Microwave Background". In: *Astronomy and Astrophysics* 107 (1982), pp. 39–42.

[42] C.-P. Ma and E. Bertschinger. "Cosmological Perturbation Theory in the Synchronous and Conformal Newtonian Gauges". In: *The Astrophysical Journal* 455 (1995), pp. 7–25. DOI: 10.1086/176550.

[43] A. Kosowsky. "Cosmic Microwave Background Polarization". In: *Annals of Physics* 246 (1996), pp. 49–85. DOI: 10.1006/aphy.1996.0020.

[44] R. Durrer. "Gauge-Invariant Cosmological Perturbation Theory for Collisionless Matter – Numerical Results". In: *Astronomy and Astrophysics* 208 (1989), pp. 1–13.

[45] J. A. Holtzman. "Microwave Background Anisotropies and Large-Scale Structure in Universes with Cold Dark Matter, Baryons, Radiation, and Massive and Massless Neutrinos". In: *The Astrophysical Journal Supplement Series* 71 (1989), pp. 1–24. DOI: 10.1086/191362.

[46] W. Hu et al. "The Effect of Physical Assumptions on the Calculation of Microwave Background Anisotropies". In: *Physical Review D* 52 (1995), pp. 5498–5515. DOI: 10.1103/PhysRevD.52.5498.

[47] Y. E. Lyubarsky and R. A. Sunyaev. "The Spectral Features in the Microwave Background Spectrum due to Energy Release in the Early Universe". In: *Astronomy and Astrophysics* 123 (1983), pp. 171–183.

[48] R. H. Cyburt et al. "Big Bang Nucleosynthesis: Present Status". In: *Reviews of Modern Physics* 88.1 (2016), p. 015004. DOI: 10.1103/RevModPhys.88.015004.

[49] V. Mukhanov. *Physical Foundations of Cosmology*. Cambridge University Press, 2005.

[50] P. J. E. Peebles. "Recombination of the Primeval Plasma". In: *The Astrophysical Journal* 153 (1968), pp. 1–11. DOI: 10.1086/149628.

[51] K. A. Malik, D. Wands, and C. Ungarelli. "Large-Scale Curvature and Entropy Perturbations for Multiple Interacting Fluids". In: *Physical Review D* 67.6 (2003), p. 063516. DOI: 10.1103/PhysRevD.67.063516.

[52] S. Weinberg. *Cosmology*. Oxford University Press, 2008.

[53] S. Weinberg. "Adiabatic Modes in Cosmology". In: *Physical Review D* 67.12 (2003), p. 123504. DOI: 10.1103/PhysRevD.67.123504.

[54] W. Hu and N. Sugiyama. "Anisotropies in the Cosmic Microwave Background: an Analytic Approach". In: *The Astrophysical Journal* 444 (May 1995), p. 489. DOI: 10.1086/175624.

[55] M. Bucher, K. Moodley, and N. Turok. "General Primordial Cosmic Perturbation". In: *Physical Review D* 62.8 (2000), p. 083508. DOI: 10.1103/PhysRevD.62.083508.

[56] J. M. Bardeen et al. “The Statistics of Peaks of Gaussian Random Fields”. In: *The Astrophysical Journal* 304 (1986), pp. 15–61. DOI: 10.1086/164143.

[57] W. H. Press and P. Schechter. “Formation of Galaxies and Clusters of Galaxies by Self-Similar Gravitational Condensation”. In: *The Astrophysical Journal* 187 (1974), pp. 425–438. DOI: 10.1086/152650.

[58] C. L. Bennett et al. “Scientific Results from COBE”. In: *Advances in Space Research* 13 (1993). DOI: 10.1016/0273-1177(93)90150-A.

[59] C. L. Bennett et al. “Nine-year Wilkinson Microwave Anisotropy Probe (WMAP) Observations: Final Maps and Results”. In: *The Astrophysical Journal Supplement* 208 (2013), p. 20. DOI: 10.1088/0067-0049/208/2/20.

[60] *Euclid Consortium*. URL: https://www.euclid-ec.org/ (visited on 04/16/2019).

[61] *Large Synoptic Survey Telescope*. URL: https://www.lsst.org/ (visited on 04/16/2019).

[62] *Wide Field Infrared Survey Telescope*. URL: https://wfirst.gsfc.nasa.gov/ (visited on 04/16/2019).

A Values of Astrophysical Parameters

This appendix lists the parameter values used in the numerical computations of section 6.2.

CMB temperature [1]

$$T_0 = 2.725\,48\,\mathrm{K}. \tag{A.1}$$

Baryon-to-photon ratio [2]

$$\eta_\mathrm{B} = 6.07 \times 10^{-10}. \tag{A.2}$$

Parameters from [3]

$$H_0 = 100\,h\,\mathrm{km\,s^{-1}\,Mpc^{-1}} \tag{A.3}$$
$$h = 0.6781 \tag{A.4}$$
$$\Omega_{\mathrm{m}0} = 0.308 \tag{A.5}$$
$$\Omega_{\Lambda 0} = 0.692 \tag{A.6}$$
$$\Omega_{\mathrm{b}0} = 0.022\,26\,h^{-2} \tag{A.7}$$
$$\Omega_{\mathrm{c}0} = 0.1186\,h^{-2}. \tag{A.8}$$

The density parameters for neutrinos and photons are computable from the CMB temperature. The energy density of photons depends on temperature as (see e.g. [4])

$$\rho_\gamma = \frac{\pi^2}{15} T^4. \tag{A.9}$$

With (A.1) and (A.3), the photon density parameter is

$$\begin{aligned} \Omega_{\gamma 0} &= \frac{\pi^2}{45} \frac{T_0^4}{M_\mathrm{p}^2 H_0^2} \\ &\approx 5.37 \times 10^{-5}. \end{aligned} \tag{A.10}$$

After the electron-positron annihilations, the neutrino energy density differs from that of photons by factor (see e.g. [4])

$$R_{\nu/\gamma} \equiv \frac{\rho_\nu}{\rho_\gamma} = \frac{21}{8} \left(\frac{4}{11}\right)^{4/3}. \tag{A.11}$$

The density parameter of neutrinos is then

$$\begin{aligned} \Omega_{\nu 0} &= R_{\nu/\gamma} \Omega_{\gamma 0} \\ &\approx 3.66 \times 10^{-5}. \end{aligned} \tag{A.12}$$

References

[1] D. J. Fixsen. "The Temperature of the Cosmic Microwave Background". In: *The Astrophysical Journal* 707 (2009), pp. 916–920. DOI: 10.1088/0004-637X/707/2/916.

[2] R. H. Cyburt et al. "Big Bang Nucleosynthesis: Present Status". In: *Reviews of Modern Physics* 88.1 (2016), p. 015004. DOI: 10.1103/RevModPhys.88.015004.

[3] Planck Collaboration. "Planck 2015 results. XIII. Cosmological Parameters". In: *Astronomy & Astrophysics* 594 (2016), A13. DOI: 10.1051/0004-6361/201525830.

[4] S. Dodelson. *Modern Cosmology*. Academic Press, 2003.

B The Python code

```
'''
Computes the evolution of perturbation variables in a
universe filled with five component (cold dark matter c,
baryons b, photons g, neutrinos n and dark energy l) real fluid.
Neutrino and photon perturbations are computed up to
second multipoles

y = 1/(1+z), z being the redshift, is used as the time variable
Figures are stored in 'fig/'.'

Made by Tuomas Aalto
Version 27.11.2018
'''

from scipy.integrate import solve_ivp
from scipy.interpolate import interp1d
import numpy as np
import matplotlib.pyplot as plt
from concurrent.futures import ProcessPoolExecutor
from itertools import repeat
from os import mkdir

plt.rcParams.update({'font.size' : 12})

# natural constants from CODATA, arXiv:1507.07956
c = 299792458               # Speed of light in m/s
alpha = 1/137.035999139     # Fine structure constant
me = 510998.9461            # Electron mass in eV
sigmat = 66.524587158       # Cross section for Thomson scattering
    in fm^2

# Present day CMB temperature in K from Fixsen 2009, arXiv
    :0911.1955
T0 = 2.72548
Omg0 = 5.37e-5              # Omega_0 for photons from T0

# Baryon-to-photon ratio from Cyburt 2015, arXiv:1505.01076
eta_bg = 6.07*10**(-10)

# Cosmological parameters from Planck 2015, arXiv:1502.01589
h = 0.6781                  # Hubble constant parameter, H0 = h*100
    (km/s)/Mpc
H0 = h*100*1000/c           # Hubble constant in Mpc^-1
Omb0 = 0.02226/h**2         # Omega_0 for baryons
Omc0 = 0.1186/h**2          # Omega_0 for CDM
```

```
43 Omm0 = 0.308                # Omega_0 for matter
44 Oml0 = 0.692                # Omega_0 for dark energy
45
46 eps0 = 13.6                 # Hydrogen ionization energy in eV
47 R_ng = 21/8*(4/11)**(4/3)   # Ratio of neutrino and photon energy
       densities
48 Omn0 = R_ng*Omg0            # Omega_0 for neutrinos
49 Omr0 = Omg0 + Omn0          # Omega_0 for radiation
50
51
52 class Quantity:
53     '''A class to specify eg. plotting details of a quantity'''
54
55     def __init__(self,symbol):
56         self.symbol = symbol
57         self.simplesymbol = ""
58         self.colindex = -1,
59         self.xlims = None,
60         self.ylims = None,
61         self.legendloc = 1
62
63
64 def iFirstSmaller(a,x):
65     '''First index i when a[i] < x'''
66     i = 0
67     while i < len(a) and a[i] > x:
68         i = i + 1
69     return i
70
71
72 def Hubble(y):
73     '''Hubble rate at y in Mpc^-1'''
74     return H0*np.sqrt(Omm0*y**(-3) + Omr0*y**(-4) + Oml0)
75
76
77 def iHorizonCrossing(k0, ys):
78     '''Index i so that scale k0 crosses horizon at ys[i]
79
80     Parameters
81     ----------
82     k0 : double
83         Scale of interest
84     ys : array of doubles
85         Time values
86
87     '''
88
89     Hy = Hubble(ys) * ys
90     return iFirstSmaller(Hy, k0)
91
92
93 def iRadEnd(tolerance, ys):
94     '''Index i so that radiation becomes a non-dominant
```

```
95      component of energy density with given tolerance at ys[i]
96
97      Parameters
98      ----------
99      tolerance : double between 0 and 1
100         Threshold determining what is considered
101         the end of radiation domination;
102         at the end of the epoch rho_rad / rho = tolerance
103     ys : array of doubles
104         Time values
105
106     '''
107
108     radiationFraction = Omr0/(Omr0 + Omm0*ys + Oml0 * ys**4)
109     return iFirstSmaller(radiationFraction, tolerance)
110
111
112 def dXedy(y,Xe):
113     '''
114     The derivative of free electron fraction with
115     respect to y from Peebles equation
116     '''
117
118     H = Hubble(y)
119     T0ineV = T0*8.6173303*10**(-5)
120     nb = eta_bg*2*1.202056903159594/np.pi**2*(T0ineV/y)**3    # in
            eV^3
121     alpha2 = 9.78*alpha*alpha*np.sqrt(eps0*y/T0ineV)*np.log(eps0*y/
            T0ineV)/me**2
122     beta = (me*T0ineV/(2*np.pi*y))**(3/2)*np.exp(-eps0*y/T0ineV)*
            alpha2
123     dimFact = 1.5637377549048648e29       # Mpc * eV
124     Lambda2s = 5.4151117694e-15
125     LambdaAlpha = ((3*eps0)**3 * H)/((8*np.pi)**2 * (1-Xe) * nb)/
            dimFact
126     beta2 = (me*T0ineV/(2*np.pi*y))**(3/2)*np.exp(-eps0*y/(4*T0ineV
            ))*alpha2
127     C = (LambdaAlpha + Lambda2s)/(LambdaAlpha + Lambda2s + beta2)
128     return C*((1-Xe)*beta - Xe*Xe*nb*alpha2)*dimFact/(H*y)
129
130
131 def XeFromSaha(y):
132     '''
133     Free electron fraction at y from Saha equation,
134     valid when near equilibrium (Xe ~ 1)
135     '''
136
137     T0ineV = T0*8.6173303e-5
138     B = np.sqrt(np.pi)*np.exp(-eps0*y/T0ineV)*(me*y/T0ineV)**(3/2)
            /(4*np.sqrt(2)*1.202056903159594*eta_bg)
139     return (np.sqrt(B*(B+4))-B)/2
140
141
```

```
142 def Xe(y):
143     '''Solve free electron fraction at y's'''
144 
145     vXeFromSaha = np.vectorize(XeFromSaha)
146     Xes = vXeFromSaha(y)
147 
148     # Determine from which index to switch from Saha eq to Peebles
        eq
149     peeblesStart = iFirstSmaller(Xes,0.99)
150 
151     Xes[peeblesStart:] = solve_ivp(
152             dXedy,
153             (y[peeblesStart],y[-1]),
154             (Xes[peeblesStart],),
155             t_eval=y[peeblesStart:],
156             method='Radau'
157         ).y[0,:]
158 
159     return Xes
160 
161 def da0etady(y,a0eta):
162     return 1/(H0*np.sqrt(Omm0*y + Omr0 + Oml0*np.power(y,4)))
163 
164 def a0eta(ys):
165     '''Solve a0 * eta at ys'''
166 
167     res = solve_ivp(
168         da0etady,
169         (ys[0],ys[-1]),
170         [ys[0]/H0/np.sqrt(Omr0)],
171         method='LSODA',
172         t_eval=ys)
173 
174     return res.y[0,:]
175 
176 def dqsdy(y,qs):
177     '''
178     Compute the derivatives of metric and fluid
179     perturbations with respect to
180     y = 1/(1+z) at y.
181 
182     Scale k0 is passed as a constant in qs, as
183     solve_ivp doesn't take additional arguments.
184 
185     Parameters
186     ----------
187     y : double
188         Timelike variable 1/(1+z), z being the redshift
189     qs : numpy array
190          Values of (Psi,
191                     deltac,vc,
192                     deltab,vb,
193                     deltag,vg,
```

```
194                     deltan,vn,
195                     Pi_g,Pi_n,
196                     k0) at y
197
198     Returns
199     -------
200     numpy array
201         Derivatives of quantities
202         Psi,deltac,vc,deltab,vb,deltag,vg,
203         deltan,vn,Pi_g,Pi_n,k0
204         where the derivative of Psi is at index 0 etc
205     '''
206
207     Psi, deltac, vc, deltab, vb, deltag, vg, deltan, vn, Pi_g, Pi_n
            , k0 = qs
208     delta = (Omg0*deltag + Omn0*deltan + Omb0*y*deltab + Omc0*y*
            deltac)/(Omg0 +
209              Omn0 + Omb0*y + Omc0*y + Oml0*y**4)
210     H = Hubble(y)
211     dimFact = 2.5698598286089585            # Mpc * fm^2 * K^3
212     nb = eta_bg*2*1.202056903159594/np.pi**2*(T0/y)**3
213     Xe = XeValuesInterp(y)
214     a0eta = a0etaValuesInterp(y)
215     # print("y: ", y, " a0eta: ", a0eta)
216     dPi_g = -(1/(H*y**2))*(4*k0*vg +
217             3*(3*nb*Xe*sigmat*dimFact*y/10 + 1/a0eta)*Pi_g)
218     dPi_n = -(1/(H*y**2))*(4*k0*vn +
219             3*Pi_n/a0eta)
220     # print("y: ", y, " a0eta: ", a0eta, " dPi_n: ", dPi_n)
221     wPi = (Omg0*Pi_g + Omn0*Pi_n)/(3*(Omr0 + Omm0*y + Oml0*y**4))
222     Phi = Psi - 3*wPi*(H*y/k0)**2
223     dPsi = -(1/y)*(Phi + (k0/(H*y))**2*Psi/3 + delta/2)
224     return (dPsi,                                   # d Psi / d y
225             k0*vc/(H*y**2) + 3*dPsi,                 # d deltac / d y
226             -k0*Phi/(H*y**2) - vc/y,                 # d vc / d y
227             k0*vb/(H*y**2) + 3*dPsi,                 # d deltab / d y
228             -vb/y - 1/(H*y**2)*(k0*Phi + 4*Omg0*nb*Xe*sigmat*(vb-vg
                )*dimFact/(3*Omb0)),  # d vb / dy
229             4*k0*vg/(3*H*y**2) + 4*dPsi,     # d deltag / dy
230             -(k0/(H*y**2))*(deltag/4 + Phi - Pi_g/6) + Xe*nb*sigmat
                *(vb-vg)*dimFact/H/y,   # d vg / d y
231             4*k0*vn/(3*H*y**2) + 4*dPsi,     # d deltan / d y
232             -(k0/(H*y**2))*(deltan/4 + Phi - Pi_n/6),  # d vn / d y
233             dPi_g,                                  # d Pi_g / d y
234             dPi_n,                                  # d Pi_n / d y
235             0                                       # d k0 / d y; scale k0
                is kept constant
236     )
237
238 def develOfK(ys, k0, i_radEnd):
239     '''
240     Compute the development of quantities Psi, deltac, vc,
241     deltab, vb, deltag, vg, deltan, vn, Pi_g, Pi_n for scale k0
```

```
        over the span ys
242
243     Parameters
244     ----------
245     ys : array like of doubles
246         Points y where quantities are evaluated
247     k0 : double
248         Scale k0 for which quantities will be computed
249     i_radEnd : int
250         Time ys[i_radEnd] at which radiation dominated
251         epoch ends
252
253     Returns
254     -------
255     dictionary with keywords
256         'k0' : double
257             k0-value for which solving was performed
258         'ys' : array like
259             Points y where quantities are evaluated
260         'vals' : numpy array
261             Solved values for the quantities
262             with Psi in column 0 etc
263
264     '''
265
266     # Determine the starting point for DE solving;
267     # quantities constant when rho ~ rho_r and k0/Hy << 1
268     kHubRatio = k0/(Hubble(ys)*ys)
269     i_kh = iFirstSmaller(-kHubRatio, -0.01)
270     solvingStarts = min((i_kh, i_radEnd))
271
272     # Initial values
273     Phi_in = 1/(2*R_ng/(5*(1+R_ng)) + 3/2)
274     v_in = -k0*Phi_in/(2*Hubble(ys[solvingStarts])*ys[solvingStarts
           ])
275     y0 = [1 - Phi_in/2,    # Psi
276           -3/2*Phi_in,     # deltac
277           v_in,  # vc
278           -3/2*Phi_in,     # deltab
279           v_in,  # vb
280           -2*Phi_in,  # deltag
281           v_in,  # vg
282           -2*Phi_in,  # deltan
283           v_in,  # vn
284           0,     # Pi_g
285           2*Phi_in/5*(k0/(Hubble(ys[solvingStarts])*ys[
                 solvingStarts]))**2,    # Pi_n
286           k0]      # k0
287
288     sol = solve_ivp(dqsdy
289                     ,(ys[solvingStarts], ys[-1])
290                     ,y0
291                     ,t_eval=ys[solvingStarts:]
```

```
292                     ,method='Radau') #
293
294     if sol.status != 0:
295         print(sol.message)
296
297     vals = np.zeros((solvingStarts + len(sol.t),11))
298
299     # Change initial conditions for varying quantities to
300     # be their values in the pre-solving regime
301     v_in_var = -k0*Phi_in/(2*Hubble(ys[0:solvingStarts])*ys[0:
            solvingStarts])
302     y0[2]  = v_in_var
303     y0[4]  = v_in_var
304     y0[6]  = v_in_var
305     y0[8]  = v_in_var
306     y0[10] = 2*Phi_in/5*(k0/(Hubble(ys[0:solvingStarts])*ys[0:
            solvingStarts]))**2  # Pi_n
307
308     # Psi in column 0, deltac in column 1,... , Pi_n in column 10
309     for i in range(0,11):
310         vals[:solvingStarts,i] = y0[i]
311         vals[solvingStarts:,i]  = sol.y[i,:]  #
312
313     return {'k0'   : k0
314             ,'ys'   : np.concatenate((ys[0:solvingStarts], sol.t))
315             ,'vals' : vals
316     }
317
318
319 def develOfKs(ys,ksOfInterest, i_radEnd):
320     '''
321     Compute the development of quantities Psi, deltac, vc, deltab,
322     vb, deltag, vg, deltan, vn, Pi_g, Pi_n for scales ksOfInterest
            over the span ys
323
324     Parameters
325     ----------
326     ys : array like of doubles
327         Points y where quantities are evaluated
328     ksOfInterest : array like of doubles
329         Scales k0 for which quantities will be computed
330     i_radEnd : int
331         Time ys[i_radEnd] at which radiation dominated
332         epoch ends
333
334     Returns
335     -------
336     list of dictionaries with keywords
337         'k0' : double
338             k0-value for which solving was performed
339         'ys' : array like of doubles
340             Points y where quantities are evaluated
341         'vals' : numpy array
```

```
342             Solved values for the quantities
343             with Psi in column 0 etc
344     '''
345
346     with ProcessPoolExecutor() as executor:
347         future = executor.map(develOfK, repeat(ys), ksOfInterest,
                repeat(i_radEnd))
348
349     return list(future)
350
351
352 def plotQuantity(data, xlims, ylims, symbol, simplesymbol,
        legendloc,
353                  loglog, y_eq_xsepf = 5e-5, y_eq_ysepf=0.05):
354     '''Make and save a (y, quantity) -plot
355
356     Parameters
357     ----------
358     data : list
359         Data to be plotted as a list of dictionarys,
360         each dictionary containing keywords:
361             'k0' : scale k0
362             'ys' : y values
363             'vals' : values of the quantity at given y values
364     xlims : 2-tuple of floats or None
365         X axis limits to be set for the plot (if any)
366     ylims : 2-tuple of floats or None
367         Y axis limits to be set for the plot (if any)
368     symbol : str
369         Symbol of the quantity
370     simplesymbol : str
371         Symbol of the quantity without Latex formatting
372     loglog : bool
373         True if both axis should be logarithmic
374     y_eq_xsepf : float
375         Separation factor in x direction between the matter-
            radiation
376         equilibrium line and its legend; 0 for legend on the line,
377         1 for legend at the right border of the plot
378     y_eq_ysepf : float
379         Separation factor in y direction between the top of the
            plot and
380         matter-radiation equilibrium legend; 0 for legend on top of
             the plot,
381         1 for legend at the bottom of the plot
382     '''
383
384     plt.gcf().clear()
385
386     i = 0
387     while i < len(data):
388         dataSingleK = data[i]
389         label = "$k_0$ = {0:.3g} Mpc$^-$$^1$".format(dataSingleK['
```

```
            k0'])
390         color = 'C' + str(i)
391         plt.plot(dataSingleK['ys']
392                 ,dataSingleK['vals']
393                 ,color + '-'
394                 ,label=label
395                 ,zorder=0
396                 )
397
398         # point where scale crosses horizon
399         try:
400             i_cross = iHorizonCrossing(dataSingleK['k0'],
                    dataSingleK['ys'])
401             quantityk = dataSingleK['vals'][i_cross]
402             plt.scatter([dataSingleK['ys'][i_cross], ]
403                         ,[quantityk, ]
404                         ,50
405                         ,color=color
406                         ,zorder=5
407                         )
408         except IndexError:
409             pass
410
411         i = i+1
412
413     if loglog:
414         plt.loglog()
415     else:
416         plt.semilogx()
417
418     try:
419         plt.xlim(xlims)
420     except:
421         pass
422     try:
423         plt.ylim(ylims)
424     except:
425         pass
426
427     plt.legend(loc=legendloc)
428
429
430     # Point of matter radiation equilibrium y_eq as a vertical line
431     y_eq = Omr0/Omm0
432     ax = plt.gca()  # [xmin,xmax,ymin,ymax]
433     plt.plot([y_eq, y_eq]
434             ,[ax.get_ylim()[0] ,ax.get_ylim()[1]]
435             ,color='black'
436             ,linewidth=1.
437             ,linestyle="--")
438     plt.annotate('$z␣=␣z_{\mathrm{eq}}$'
439                 ,(y_eq + y_eq_xsepf*(ax.get_xlim()[1] - ax.get_xlim
                        ()[0])
```

```
440                 ,ax.get_ylim()[1] - y_eq_ysepf*(ax.get_ylim()[1] -
                        ax.get_ylim()[0]))
441                 )
442
443     plt.ylabel(symbol + ' ($\mathcal{R}_{\mathrm{prim}}$)')
444     plt.xlabel('$(1+z)^{-1}$')
445
446     # Save the figure
447     plt.savefig("fig/" + simplesymbol + ".pdf", dpi=144)
448
449
450 if __name__ == '__main__':
451     Psi = Quantity('$\Psi$')
452     Psi.simplesymbol = "Psi"
453     Psi.colindex = 0
454     Psi.ylims = (-0.2, 0.9)
455     Psi.legendloc = 3
456
457     deltac = Quantity('$\delta_\mathrm{c}$')
458     deltac.simplesymbol = "deltac"
459     deltac.colindex = 1
460     deltac.ylims = (-100,10)
461     deltac.legendloc = 3
462
463     vc = Quantity('$v_\mathrm{c}$')
464     vc.simplesymbol = "vc"
465     vc.colindex = 2
466     vc.ylims = (-20,5)
467     vc.legendloc = 3
468
469     deltab = Quantity('$\delta_\mathrm{b}$')
470     deltab.simplesymbol = "deltab"
471     deltab.colindex = 3
472     deltab.ylims = (-100,15)
473     deltab.legendloc = 3
474
475     vb = Quantity('$v_\mathrm{b}$')
476     vb.simplesymbol = "vb"
477     vb.colindex = 4
478     vb.ylims = (-20,5)
479     vb.legendloc = 3
480
481     deltag = Quantity('$\delta_\mathrm{\gamma}$')
482     deltag.simplesymbol = "deltag"
483     deltag.colindex = 5
484     deltag.ylims = (-5,5)
485     deltag.legendloc = 2
486
487     vg = Quantity('$v_\mathrm{\gamma}$')
488     vg.simplesymbol = "vg"
489     vg.colindex = 6
490     vg.ylims = (-2.3,2.3)
491     vg.legendloc = 2
```

```
492
493     deltan = Quantity('$\delta_\mathrm{\\nu}$')
494     deltan.simplesymbol = "deltan"
495     deltan.colindex = 7
496     deltan.ylims = (-5,1.5)
497     deltan.legendloc = 2
498
499     vn = Quantity('$v_\mathrm{\\nu}$')
500     vn.simplesymbol = "vn"
501     vn.colindex = 8
502     vn.ylims = (-2,2)
503     vn.legendloc = 2
504
505     Pi_g = Quantity('$\Pi_\mathrm{\\gamma}$')
506     Pi_g.simplesymbol = "Pi_g"
507     Pi_g.colindex = 9
508     Pi_g.ylims = (-2,2)
509     Pi_g.legendloc = 3
510
511     Pi_n = Quantity('$\Pi_\mathrm{\\nu}$')
512     Pi_n.simplesymbol = "Pi_n"
513     Pi_n.colindex = 10
514     Pi_n.ylims = (-4.5,1.5)
515     Pi_n.legendloc = 3
516
517     quantities = [Psi,
518                   deltac,
519                   vc,
520                   deltab,
521                   vb,
522                   deltag,
523                   vg,
524                   deltan,
525                   vn,
526                   Pi_g,
527                   Pi_n
528                   ]
529
530     for qty in quantities:
531         qty.xlims = (1e-9, 1)
532
533     ksOfInterest = [2, 0.1, 0.003, 0.0005]
534     ys = np.logspace(-13,0,50000)
535
536     # Solve free electron fraction and save its plot
537     XeValues = Xe(ys)
538     XeValuesInterp = interp1d(ys, XeValues,kind='cubic',fill_value=
            'extrapolate')
539
540     plt.gcf().clear()
541     plt.plot(ys, XeValues)
542     plt.loglog()
543     plt.ylim((5e-5, 5e0))
```

```
544     plt.xlim((1e-9,1))
545     plt.ylabel('X$_{\mathrm{e}}$')
546     plt.xlabel('$(1+z)^{-1}$')
547     try:
548         plt.savefig("fig/Xe.pdf", dpi=144)
549     except FileNotFoundError:
550         mkdir("fig")
551         plt.savefig("fig/Xe.pdf", dpi=144)
552 
553     # Solve a0 * eta (present day scale factor times conformal time
        )
554     # and save its plot
555     a0etaValues = a0eta(ys)
556     a0etaValuesInterp = interp1d(ys,a0etaValues,kind='cubic',
        fill_value='extrapolate')
557 
558     plt.gcf().clear()
559     plt.plot(ys, a0etaValues)
560     plt.loglog()
561     plt.ylabel('$a_0\eta$')
562     plt.xlabel('$(1+z)^{-1}$')
563     try:
564         plt.savefig("fig/a0eta.pdf", dpi=144)
565     except FileNotFoundError:
566         mkdir("fig")
567         plt.savefig("fig/a0eta.pdf", dpi=144)
568 
569     # Point y at which radiation domination starts to phase out
570     i_radEnd = iRadEnd(0.95, ys)
571 
572     # Solve other quantities
573     res = develOfKs(ys,ksOfInterest, i_radEnd)
574 
575     # Plot Phi = Psi - 3*w*Pi*(H*y/k0)^2
576     phiData = []
577     for result in res:
578         y = result['ys']
579         k0 = result['k0']
580         H = Hubble(y)
581         wPi = (Omg0*result['vals'][:,Pi_g.colindex] + Omn0*result['
            vals'][:,Pi_n.colindex])/(3*(Omr0 + Omm0*y + Oml0*y**4))
582         Phi = result['vals'][:,Psi.colindex] - 3*wPi*(H*y/k0)**2
583         phiData.append({'k0'   : k0
584                        ,'vals' : Phi
585                        ,'ys'   : y
586         })
587 
588     plotQuantity(phiData
589                 ,(1e-9,1)
590                 ,(-0.2,0.8)
591                 ,'$\Phi$'
592                 ,'Phi'
593                 ,3
```

```
594                 ,False)
595
596     # Save the plots of the rest of the quantities
597     for qnty in quantities:
598         data = []
599         for result in res:
600             data.append({'k0' : result['k0']
601                         ,'vals' : result['vals'][:,qnty.colindex]
602                         ,'ys' : result['ys']
603             })
604
605         plotQuantity(data
606                     ,qnty.xlims
607                     ,qnty.ylims
608                     ,qnty.symbol
609                     ,qnty.simplesymbol
610                     ,qnty.legendloc
611                     ,False)
612
613     # Save a loglog plot of matter density contrasts
614     for qnty in [deltab,deltac]:
615         data = []
616         for result in res:
617             data.append({'k0' : result['k0']
618                         ,'vals' : np.abs(result['vals'][:,qnty.
                                colindex])
619                         ,'ys' : result['ys']
620             })
621
622         plotQuantity(data
623                     ,qnty.xlims
624                     ,[6e-1,100000]
625                     ,"|" + qnty.symbol + "|"
626                     ,"abs_" + qnty.simplesymbol + "_loglog"
627                     ,2
628                     ,True
629                     ,y_eq_ysepf=0.5)
```